RECENT MÖSSBAUER STUDIES ON MFe_2O_4 AND $M_xN_{1-x}Fe_2O_4$ FERRITES, WITH M, N = Ni, Zn, Mg

César A. Barrero Meneses, Harrison O. Salazar Tamayo, Luisa F. Vargas Restrepo, Karen E. García Tellez. **Universidad de Antioquia, Colombia**

Carlos A. Palacio-Gómez. **Universidad Antonio Nariño, Colombia**

Juan A. Jaén. **Universidad de Panamá, Panama**

LACAME'22
XVII Latin American Conference On The Applications Of The Mössbauer Effect

CONTENT

1. Ferrites with spinel structure
2. Recoilless *f*-factor for MFe_2O_4; M = Fe, Ni, Mg
3. $Ni_{1-x}Zn_xFe_2O_4$
4. $Mg_{1-x}Zn_xFe_2O_4$

1. FERRITES WITH SPINEL STRUCTURE

Spinel structure

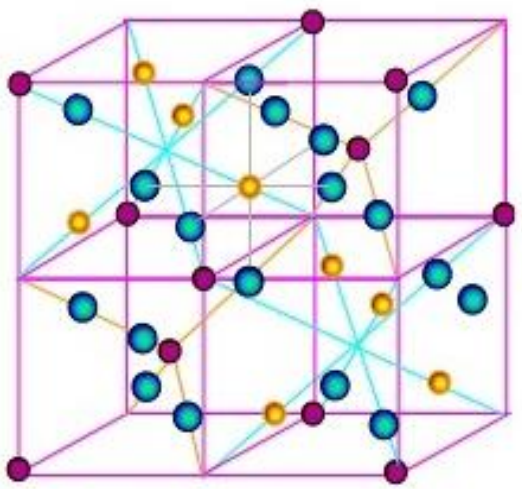

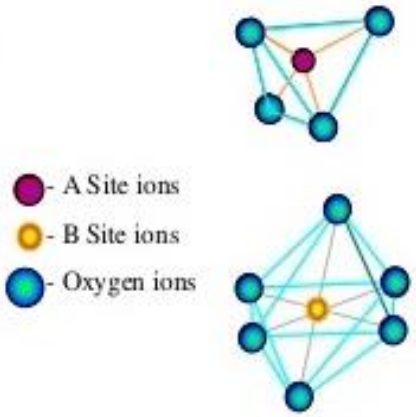

Tetrahedral site

Octahedral site

Cubic system
Space group: Fd-3m

Chemical formula

MFe_2O_4

M are chemical elements with oxidation state +2

$$(M^{2+}_{1-\lambda}\ Fe^{3+}_{\lambda})_A\ [M^{2+}_{\lambda}\ Fe^{3+}_{2-\lambda}]_B\ O^{2-}_4$$

λ: inversion degree $0 \leq \lambda \leq 1$

( ): tetrahedral sites (A-sites)

[ ]: octahedral sites [B-sites]

Classification of spinel structure

Normal Spinel

$$(M^{2+})_A\ [Fe_2^{3+}]_B\ O_4^{2-}$$

Divalent cations M^{2+} occupy tetrahedral sites, trivalent cations Fe^{3+} occupy octahedral sites.

$$\lambda = 0$$

Inverse Spinel

$$(Fe^{3+})_A\ [M^{2+}\ Fe^{3+}]_B\ O_4^{2-}$$

Divalent cations M^{2+} occupy octahedral sites, trivalent cations Fe^{3+} occupy tetrahedral and octahedral sites.

$$\lambda = 1$$

Mixed Spinel

$$(\ M_{1-\lambda}^{2+}\ Fe_{\lambda}^{3+}\ )_A\ [\ M_{\lambda}^{2+}\ Fe_{2-\lambda}^{3+}\ ]_B\ O_4^{2-}$$

M^{2+} and Fe^{3+} occupy tetrahedral and octahedral sites simultaneously and in different proportions.

$$0< \lambda <1$$

Quaternary ferrites

$M_xN_{1-x}Fe_2O_4$ (M, N = Fe, Ni, Zn, Mg)

$(Fe_{1-x}M_x)[N_{1-x}Fe_{1+x}]O_4$

$(N_{\xi x}M_{\eta(1-x)}\,Fe_{1-\xi x-\eta(1-x)})[N_{(1-\,\xi)x}M_{(1-\eta)(1-x)}Fe_{1+\xi x+\eta(1-x)}]O_4$

$(N_\alpha M_{x-\beta}Fe_{1-x+\gamma})[N_{1-x-\alpha}M_\beta Fe_{1+x-\gamma}]O_4$

$(N_{\alpha x}M_{(1-x)\beta}Fe_{2\lambda})[N_{x(1-\alpha)}M_{(1-x)(1-\beta)}Fe_{2-2\lambda}]O_4$

Properties

Superficial area

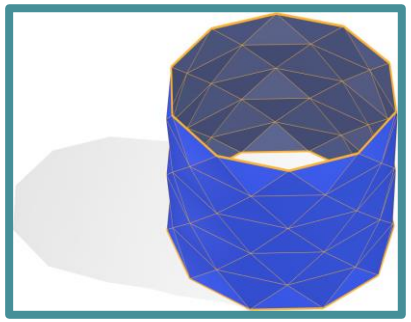

Reactivity

Reversible adsorption

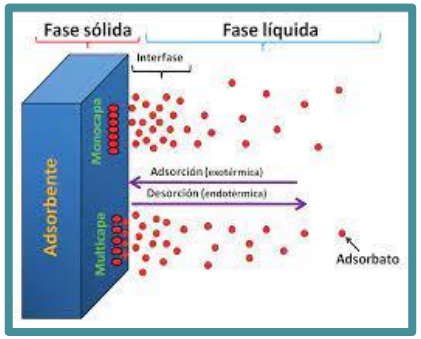

Particle size

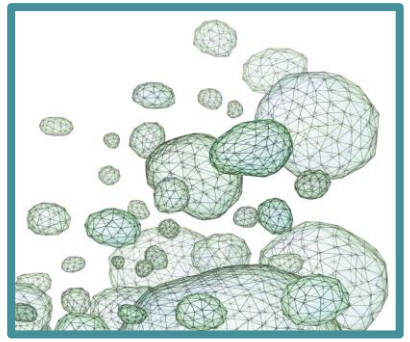

Magnetic separation

D.E. Giles, M. Mohapatra, T.B Issa, S. Anand, P. Singh. *Iron and aluminium based adsorption strategies for removing arsenic from water.* Journal of Environmental Management 92 (2011) 3011–3022.

2. RECOILLESS *f*-FACTOR for MFe_2O_4; M = Fe, Ni, Mg

The **recoilless *f*-factor** is the fraction of gamma rays which are emitted and absorbed without recoil.

$$f = e^{-k^2\langle x^2\rangle}$$

Debye model for lattice vibrations

$$f = exp\left\{-\left(\frac{3E_R}{2k_B\theta_D}\right)\left[1+\left(\frac{2T}{\theta_D}\right)^2\int_0^{\theta_D/T}\frac{x}{e^x-1}dx\right]\right\}$$

The recoilless *f*-factor is closely related with the atomic vibrations in the solid in which the Mössbauer nucleus is embedded and allows determination of relative atomic, molecular or weight fractions of iron compounds in the absorber.

Subspectral area ratio method

For uniform and nonpolarizing absorbers (Transmission Integral):

$$N(E) = BG + \eta_M f_s \frac{2}{\pi\Gamma_0} \int_{-\infty}^{+\infty} d\psi \frac{\Gamma_0^2/4}{(\psi + E)^2 + \Gamma_0^2/4} \left(e^{-\sigma_a' \psi} - 1\right)$$

where $$\sigma_a'(E) = \sum_i f_{a,i} n_{a,i} \sigma_{a,i}(E)$$

In the thin absorber approximation:

$$N_{th}(E) = BG - \eta_M f_s \frac{2}{\pi\Gamma_0} \sum_i f_{a,i} n_{a,i} \int_{-\infty}^{+\infty} d\psi \frac{\Gamma_0^2/4}{(\psi + E)^2 + \Gamma_0^2/4} \sigma_{a,i} \psi$$

The total spectral area is given by:

$$A_T = \int_{-\infty}^{+\infty} dE[BG - N_{th}(E)] = \sum_i \frac{\pi}{2} \sigma_0 \Gamma_0 \eta_M f_s f_{a,i} n_{a,i}$$

Margulies, Ehrman. *Nucl. Instrum. Methods Phys. Res.* 12 (1961) 131
Rancourt, McDonald, Lalonde, Ping. *Am. Miner.* 78 (1993) 1
Vandenberghe, De Grave, de Bakker. *Hyperfine Interact.* 83 (1994) 29

Subspectral area ratio method

$$A_T = \sum_i A_i = \sum_i \frac{\pi}{2}\sigma_0 \Gamma_0 \eta_M f_s f_{a,i} n_{a,i}$$

Absorber made of homogeneous mixture of compound, *i*, and reference, *r*:

$$\frac{A_i}{A_r} = \frac{\frac{\pi}{2}\sigma_0 \Gamma_0 \eta_M f_s f_{a,i} n_{a,i}}{\frac{\pi}{2}\sigma_0 \Gamma_0 \eta_M f_s f_{a,r} n_{a,r}} = \frac{f_{a,i} n_{a,i}}{f_{a,r} n_{a,r}}$$

$$n_{a,j} = \frac{N_A m_{a,j} a O_{a,j} N_{a,j}}{\mu_{a,j} A}$$

ONE relative *f*-factor ⟶

$$\frac{f_i}{f_r} = \left(\frac{m_r}{m_i}\right)\left(\frac{\mu_i}{\mu_r}\right)\left(\frac{A_i}{A_r}\right)$$

σ_0: cross-section at resonance
Γ_0: FWHM of Mössbauer transition
η_M: Mössbauer gamma of BG
f: recoilless *f*-factor
n: total number of ^{57}Fe per cm^2.
N_A: Avogadro number
m: mass
a: ^{57}Fe natural abundance
O: iron occupancy factor
N: number of Fe per formula unit
μ: molar weight
A: spectral área

Oh, Cook. *J. Appl. Phys.* 85 (1999) 32
Sorescu. *Materials Letters 54* (2002) 256
Sorescu. *J. Nanoparticle Res. 4* (2002) 221

Extension of the area ratio method

The subspectral area ratio method at a single *T* assumes that there is only ONE average *f*-factor value for irons at all sites in the compound. Therefore, we will call this method the **One relative *f*-factor.**

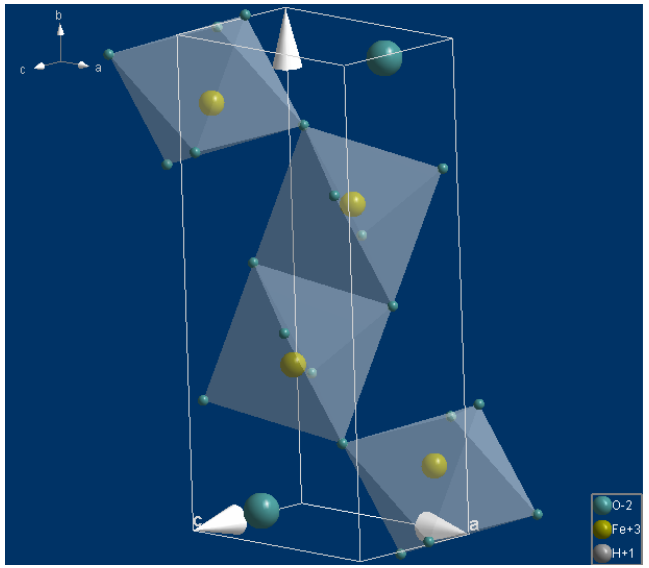

Fe^{3+} at one crystallographic site

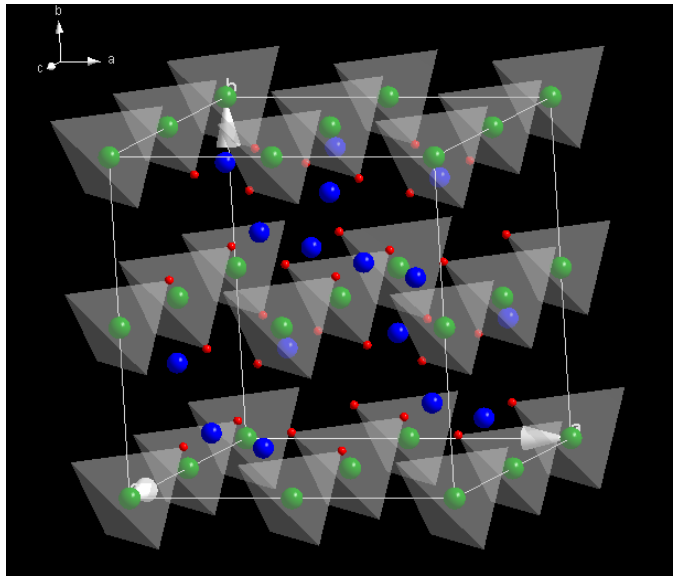

Fe^{3+} at two crystallographic sites

¿Is it possible to extend this subspectral area method to determine simultaneously **TWO relative *f*-factors,** associated to two iron sites in the compound?

Extension of the area ratio method

Total spectral area → $A_T = A_1 + A_2 + A_r$

$$\frac{A_1}{A_r} + \frac{A_2}{A_r} = \frac{A_T}{A_r} - 1$$

Spectral area of site *i*. → $A_i = \pi/2\,\sigma_0 \Gamma_0 \eta_M f_s f_{a,i} n_{a,i}$

Combination of previous equations →

$$\frac{n_1 f_1}{n_r f_r} + \frac{n_2 f_2}{n_r f_r} = \frac{A_T}{A_r} - 1$$

Sum of $^{57}Fe/cm^2$ thicknesses of two Fe sites → $n_1 + n_2 = n_{compound}$

fraction *y* (or 1-*y*) of Fe atoms in the compound are located in site 1 (or 2). → $n_1 = y n_{compound}$ $n_2 = (1-y) n_{compound}$

$^{57}Fe/cm^2$ thicknesses of a compound.

$$n_{compound} = \frac{N_A m_{compound} aO_{compound} N_{compound}}{\mu_{compound} A}$$

Barrero & Garcia, *Journal of Chemical Physics* 139 (2013) 034703.

Magnetite

Mixture of magnetite ($Fe_{3-x}O_4$) and iron powder

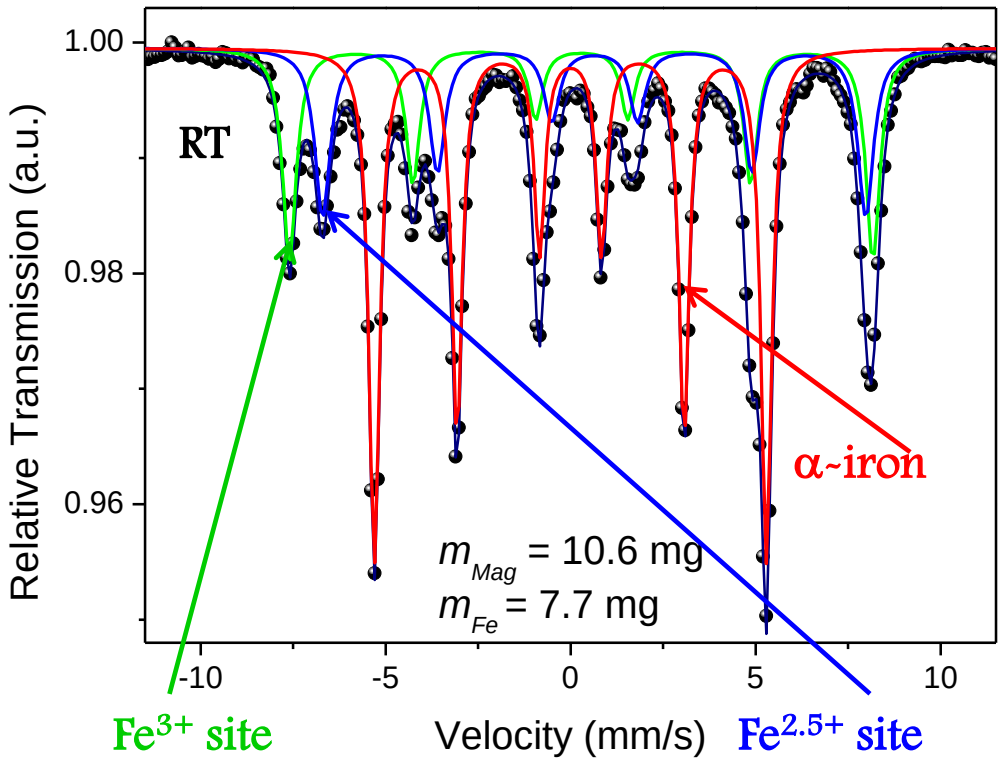

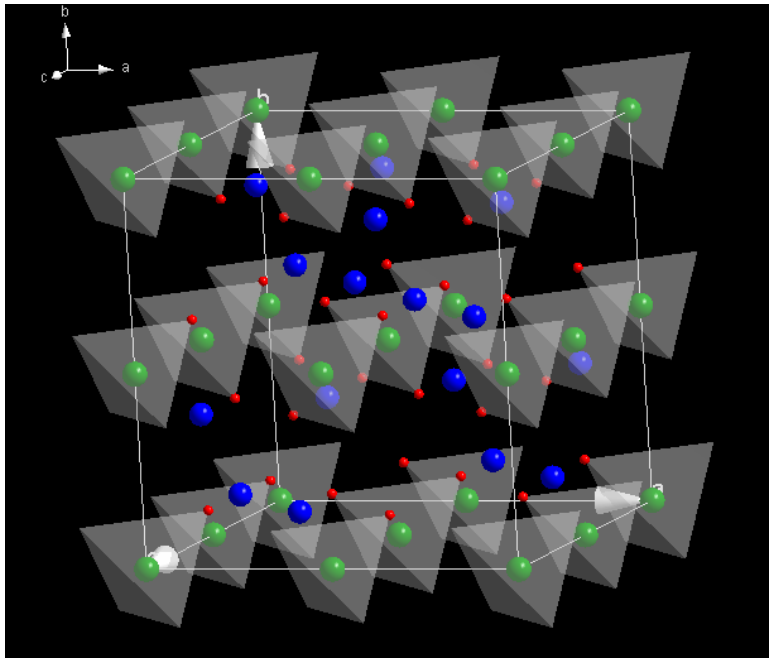

$$(Fe^{3+})_{Tetra}[Fe^{2.5+}_{2(1-3x)}Fe^{3+}_{5x}\square_x]_{Octa}O^{2-}_4$$

$$\frac{f_{Fe^{3+}}}{f_{Fe}} = \left(\frac{1}{1+5x}\right)\left(\frac{\mu_{Mag}}{\mu_{Fe}}\right)\left(\frac{m_{Fe}}{m_{Mag}}\right)\left(\frac{\frac{A_T}{A_{Fe}}-1}{\frac{A_{Fe^{2.5+}}}{A_{Fe^{3+}}}+1}\right)$$

$$\frac{f_{Fe^{2.5+}}}{f_{Fe}} = \left(\frac{1}{2-6x}\right)\left(\frac{\mu_{Mag}}{\mu_{Fe}}\right)\left(\frac{m_{Fe}}{m_{Mag}}\right)\left(\frac{\frac{A_T}{A_{Fe}}-1}{\frac{A_{Fe^{3+}}}{A_{Fe^{2.5+}}}+1}\right)$$

Barrero & Garcia, *Journal of Chemical Physics* 139 (2013) 034703.

Masses of magnetite (m_{Mag}) and iron powder (m_{Fe}). Relative spectral areas A_{Fe}^{3+}, $A_{Fe}^{2.5+}$, A_{Fe} and f-factors f_{Fe}^{3+}, $f_{Fe}^{2.5+}$, f_{Fe} for Fe^{3+} and $Fe^{2.5+}$ sites of magnetite and iron powder, respectively. [$m_{Thin} < m_{Mag}$, $m_{Fe} < m_{Ideal}$].

m_{Mag} (mg)	m_{Fe} (mg)	A_{Fe}	A_{Fe}^{3+}	$A_{Fe}^{2.5+}$	f_{Fe}^{3+}/f_{Fe}	$f_{Fe}^{2.5+}/f_{Fe}$
5.9	4.4	54.8	22.1	23.1	0.90	0.85
7.1	5.2	53.0	22.4	24.6	0.95	0.90
8.8	6.4	51.0	23.4	25.6	1.02	0.96
13.6	9.9	51.7	23.5	24.8	0.99	0.94

$f_{Fe}^{3+}/f_{Fe} = 0.97 \pm 0.05$, $f_{Fe}^{2.5+}/f_{Fe} = 0.92 \pm 0.05$; and $f_{Fe}^{2.5+}/f_{Fe}^{3+} = 0.95 \pm 0.05$

$f_{Fe}^{2.5+}/f_{Fe}^{3+} = 0.94 \pm 0.02$ reported by *Sawatzky et al., Phys. Rev.* **183** (1969) 383 .

Nickel ferrite

Mixture of $NiFe_2O_4$ and iron powder

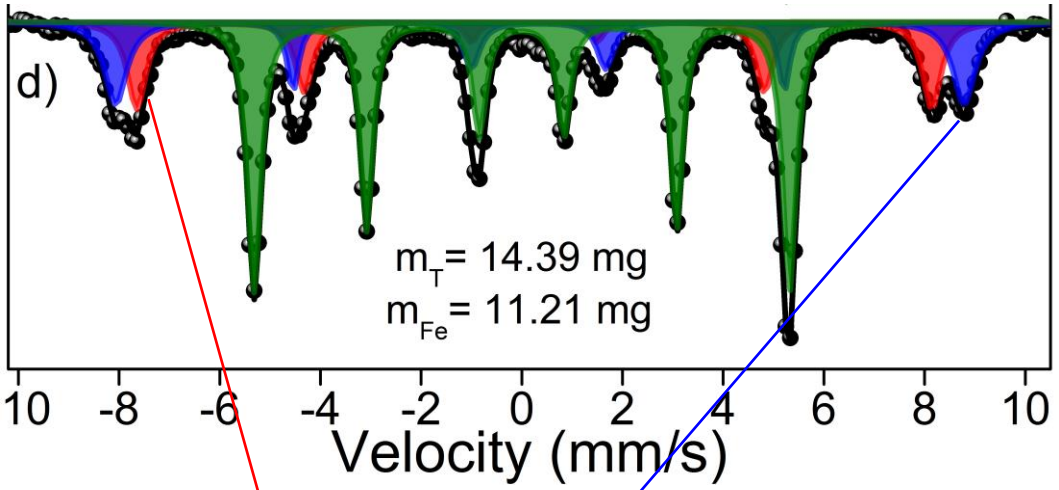

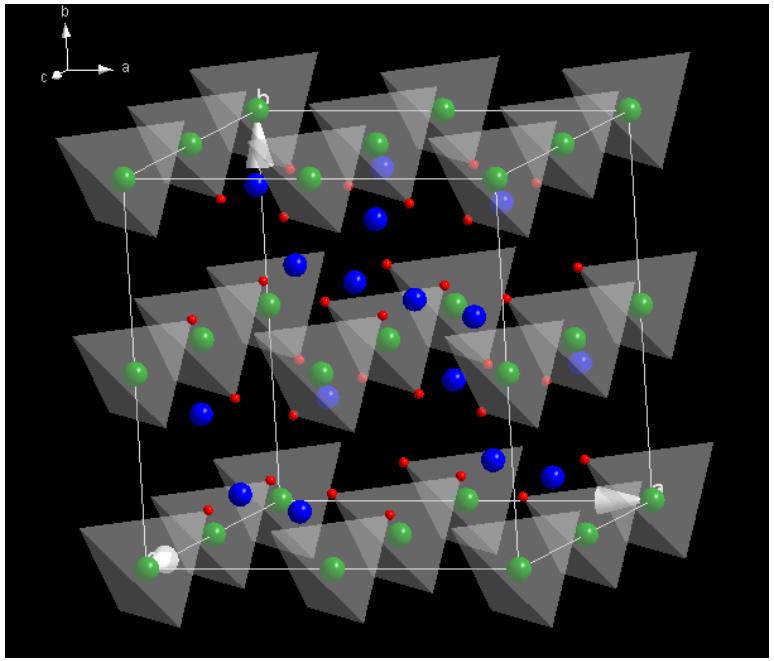

$$(Ni^{2+}_{1-\lambda}Fe^{3+}_{\lambda})_A\,[Ni^{2+}_{\lambda}Fe^{3+}_{2-\lambda}]_B\,O^{2-}_4$$

$$\frac{f_{Fe_A^{3+}}}{f_{Fe}} = \left(\frac{1}{\lambda}\right)\left(\frac{m_{Fe}}{m_T}\right)\left(\frac{\mu_T}{\mu_{Fe}}\right)\frac{\left(\frac{A_M}{A_{Fe}}-1\right)}{\left(\frac{A_{Fe_B^{3+}}}{A_{Fe_A^{3+}}}+1\right)}$$

$$\frac{f_{Fe_B^{3+}}}{f_{Fe}} = \left(\frac{1}{2-\lambda}\right)\left(\frac{m_{Fe}}{m_T}\right)\left(\frac{\mu_T}{\mu_{Fe}}\right)\frac{\left(\frac{A_M}{A_{Fe}}-1\right)}{\left(\frac{A_{Fe_A^{3+}}}{A_{Fe_B^{3+}}}+1\right)}$$

Lagarec, Rancourt, Recoil: Mössbauer Spectral Analysis Software for Windows, version 1.0 (University of Ottawa, Canada, 1998).

Salazar-Tamayo, García, Barrero, *J. Magn. Magn. Mater.* 471 (2019) 242

Determination of degree of inversion

$$a_{th} = \frac{8}{3\sqrt{3}}[(r_A + R_0) + \sqrt{3}(r_B + R_0)]$$

$$r_A = ((1-\lambda)r_{Ni^{2+}} + \lambda r_{Fe^{3+}})$$

$$r_B = \frac{1}{}[\lambda r_{Ni^{2+}} + (2-\lambda)r_{Fe^{3+}}]$$

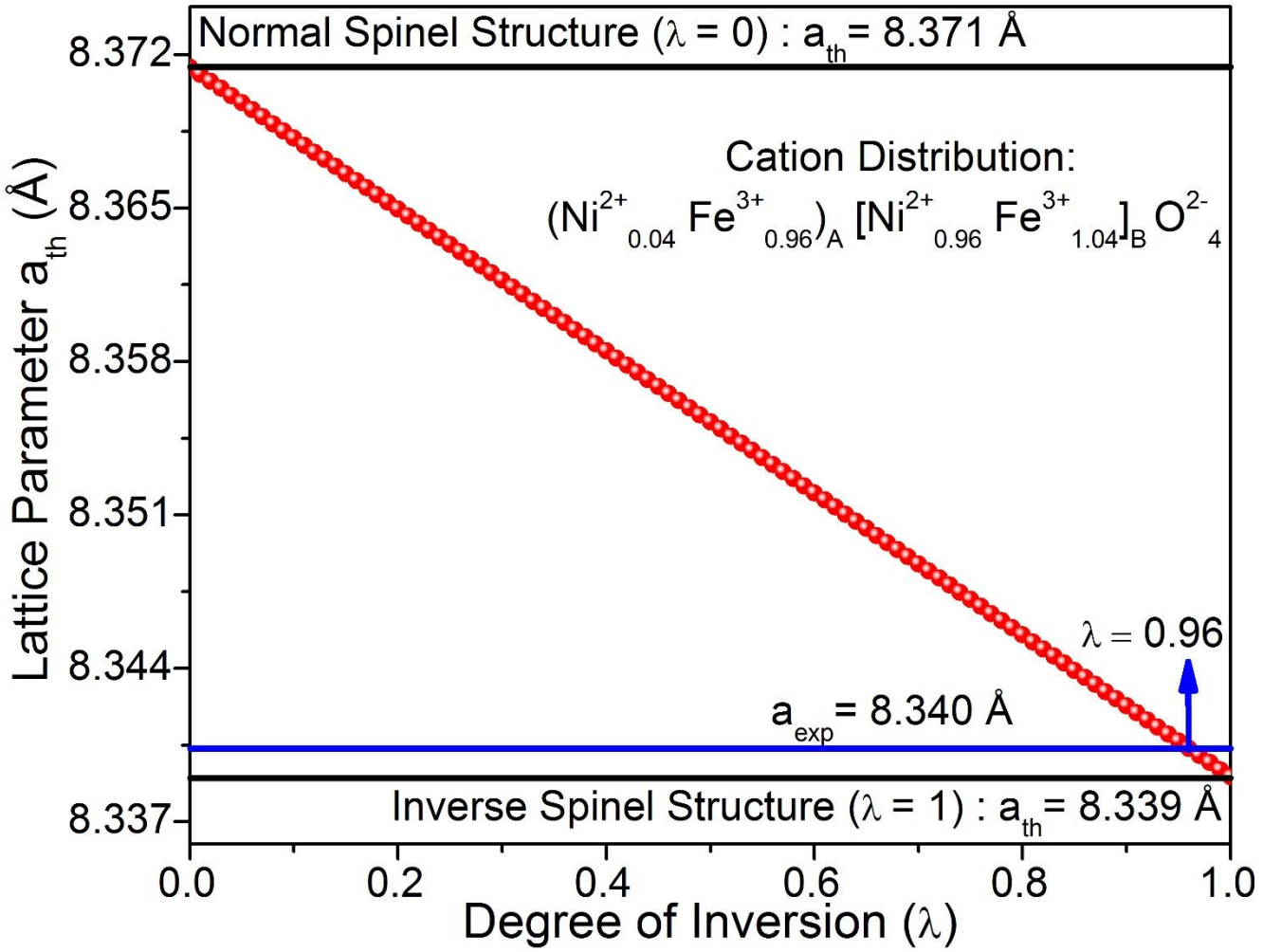

Salazar-Tamayo, García, Barrero, *J. Magn. Magn. Mater.* 471 (2019) 242

300 K thickness-corrected Mössbauer spectra of the homogeneous mixtures of $NiFe_2O_4$ and metallic iron powder. The masses are indicated in each spectrum.

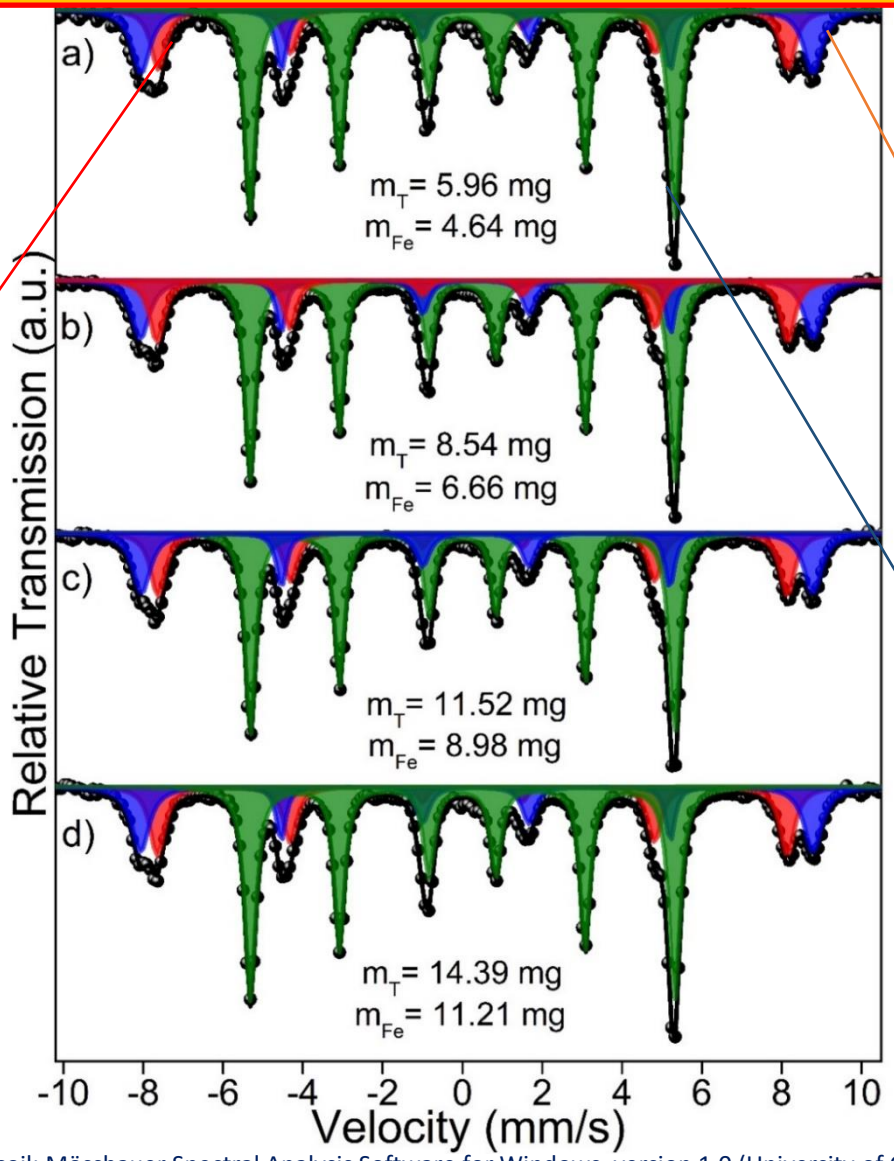

Fe_A^{3+}

Fe_B^{3+}

Metallic iron powder

Lagarec, Rancourt, Recoil: Mössbauer Spectral Analysis Software for Windows, version 1.0 (University of Ottawa, Canada, 1998).

Salazar-Tamayo, García, Barrero, *J. Magn. Magn. Mater.* 471 (2019) 242

Masses of the $NiFe_2O_4$ (m_T) and metallic Fe (m_{Fe}) materials used in the Mössbauer absorbers.

Sample code	m_T (mg)	m_{Fe} (mg)
a)	5.96	4.64
b)	8.54	6.66
c)	11.52	8.98
d)	14.39	11.21

Spectral areas and Mössbauer recoilless *f*-factors of the (A) and [B] sites of $NiFe_2O_4$. A_{Fe} and f_{Fe} are the spectral area and the Mössbauer recoilless *f*-factor of the metallic Fe powder.

Sample	$A_{Fe_A^{3+}}$	$A_{Fe_B^{3+}}$	A_{Fe}	$\frac{f_{Fe_A^{3+}}}{f_{Fe}}$	$\frac{f_{Fe_B^{3+}}}{f_{Fe}}$	$f_{Fe_A^{3+}}$	$f_{Fe_B^{3+}}$	$\frac{f_{Fe_B^{3+}}}{f_{Fe_A^{3+}}}$
a)	20.1	23.7	56.2	1.22	1.33	0.85	0.93	1.09
b)	20.0	23.4	56.6	1.20	1.30	0.84	0.91	1.08
c)	19.9	23.7	56.4	1.20	1.32	0.84	0.93	1.10
d)	20.1	23.6	56.3	1.22	1.32	0.85	0.92	1.08

$$\frac{f_{Fe_B^{3+}}}{f_{Fe_A^{3+}}} = 1.09 \pm 0.01$$

Salazar-Tamayo, García, Barrero, *J. Magn. Magn. Mater.* 471 (2019) 242

Magnesium ferrite

Mixture of $MgFe_2O_4$ and iron powder

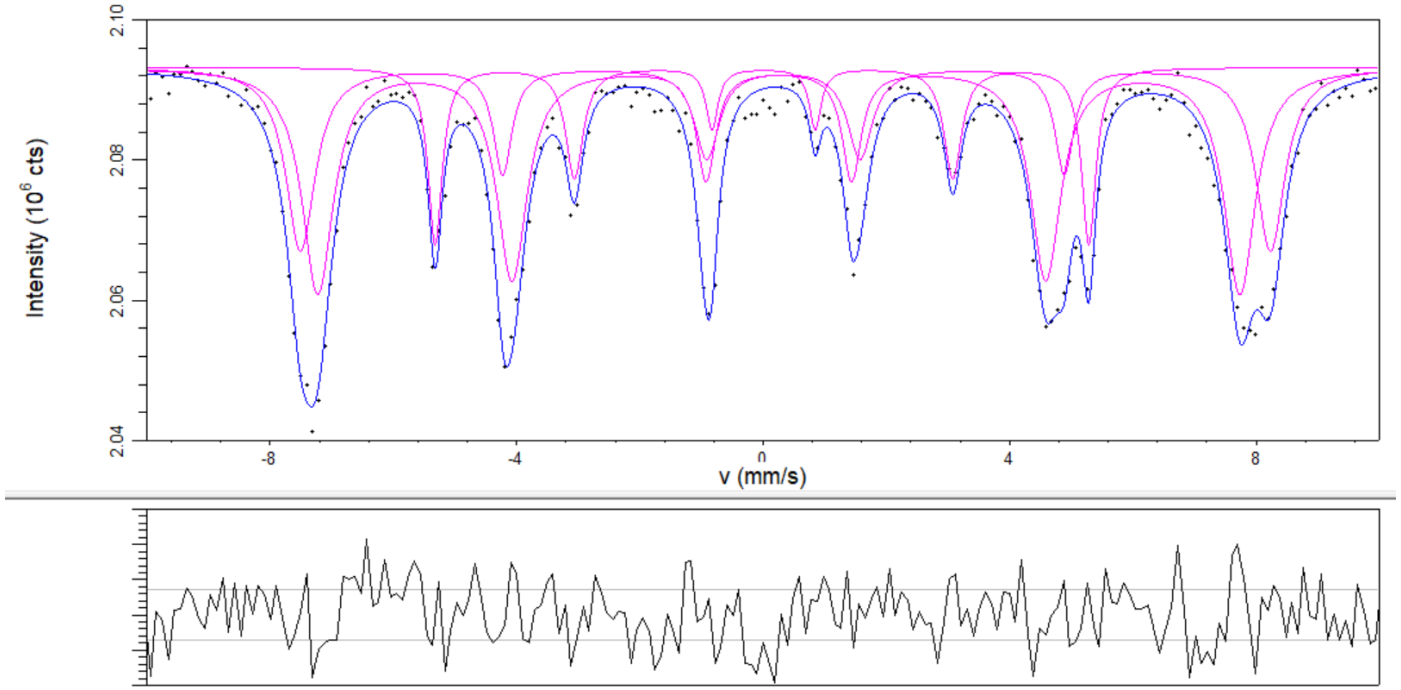

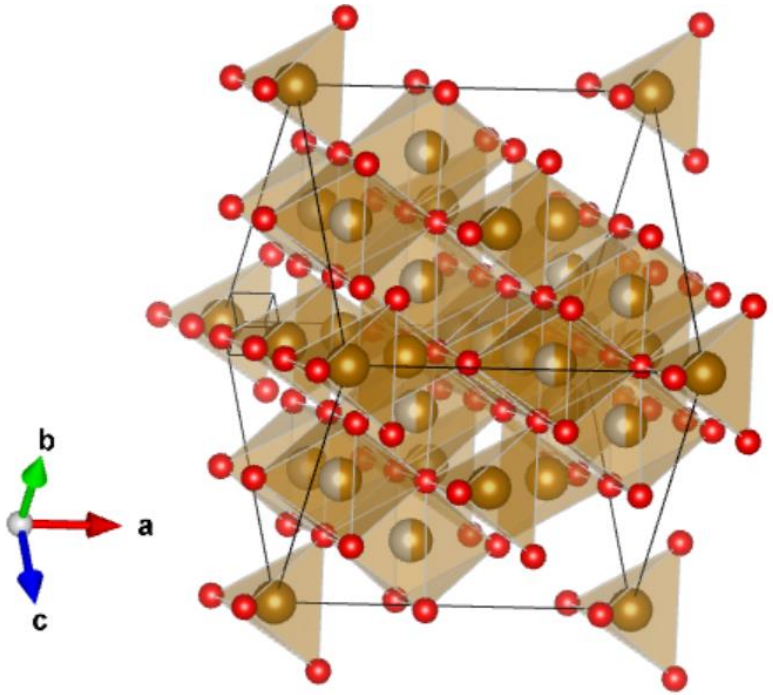

$$(Mg_{1-\lambda} Fe_{\lambda})_A [Mg_{\lambda} Fe_{2-\lambda}]_B O_4$$

$$\frac{f_{Fe_A^{3+}}}{f_{Fe}} = \left(\frac{1}{\lambda}\right)\left(\frac{m_{Fe}}{m_T}\right)\left(\frac{\mu_T}{\mu_{Fe}}\right)\frac{\left(\frac{A_M}{A_{Fe}}-1\right)}{\left(\frac{A_{Fe_B^{3+}}}{A_{Fe_A^{3+}}}+1\right)}$$

$$\frac{f_{Fe_B^{3+}}}{f_{Fe}} = \left(\frac{1}{2-\lambda}\right)\left(\frac{m_{Fe}}{m_T}\right)\left(\frac{\mu_T}{\mu_{Fe}}\right)\frac{\left(\frac{A_M}{A_{Fe}}-1\right)}{\left(\frac{A_{Fe_A^{3+}}}{A_{Fe_B^{3+}}}+1\right)}$$

The RT recoilless f-factor ratio of $f_{Fe^{3+},A}/f_{Fe}$ and $f_{Fe^{3+}B}/f_{Fe}$ were 0.91 and 1.38, respectively.
Quotient of these two *f*-factors $f_{Fe^{3+}B}/f_{Fe^{3+}A}$ is equal to 1.51.

3. $Ni_{1-x}Zn_xFe_2O_4$ (x = 0)

Cation Vacancies in $NiFe_2O_4$ During Heat Treatments

(a) Mixture NiO and α-Fe_2O_3
(b) 1000 °C
(c) 1100 °C
(d) 1200 °C.

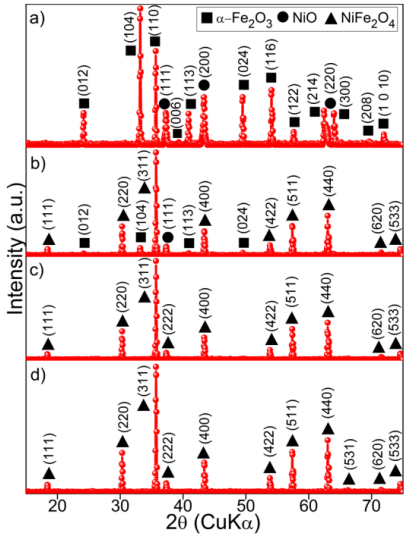

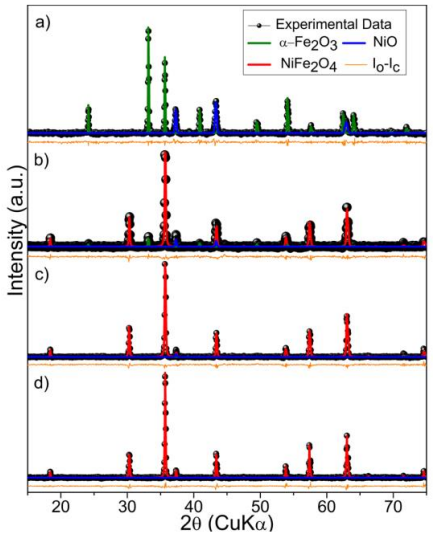

$$a_{th} = a_0 + m\,\lambda \quad (1)$$

in which λ is the inversion parameter, and:

$$a_0 = \frac{8}{3\sqrt{3}}\left[r_{Ni_A^{2+}} + (\sqrt{3})r_{Fe_B^{3+}} + (1+\sqrt{3})R_0\right] = 8.371\ \text{Å} \quad (2)$$

$$m = \frac{8}{3\sqrt{3}}\left[-r_{Ni_A^{2+}} + \left(\frac{\sqrt{3}}{2}\right)r_{Ni_B^{2+}} + r_{Fe_A^{3+}} - \left(\frac{\sqrt{3}}{2}\right)r_{Fe_B^{3+}}\right] = -0.032\ \text{Å} \quad (3)$$

8.339 Å (λ = 1) ≤ a_{th} ≤ 8.371 Å (λ = 0)

Table 1. Variation with temperature of the relative abundances and of the lattice parameter of $NiFe_2O_4$. The conventional statistical parameters χ^2, R_{wp} and R_{exp} were obtained from the Rietveld analysis of the XRD patterns. Estimated errors are of about 1 wt. % for the phase abundances and of 0.001 Å for the lattice parameters.

Sample	NiO (wt.%)	α-Fe_2O_3 (wt.%)	$NiFe_2O_4$ (wt.%)	*a* (Å) ($NiFe_2O_4$)	R_{wp} (%)	R_{exp} (%)	χ^2
Initial mixture	32	68	---	---	9.23	7.65	1.46
1000 °C	6	13	81	8.333	8.46	7.11	1.42
1100 °C	< 1*	< 2*	97	8.336	7.27	6.35	1.31
1200 °C	---	---	100	8.340	7.65	6.58	1.35

*Values below or near to the XRD detection limit.

Table 2. Hyperfine parameters for the (A) and [B] sites of $NiFe_2O_4$. δ_A and δ_B are the isomer shifts, $2_{\varepsilon A}$ and $2_{\varepsilon B}$ are the quadrupole shifts, B_A and B_B are the hyperfine magnetic fields, and A_A and A_B are the relative spectral areas for irons at (A) and [B] sites, respectively.

Sample	δ_A (mm/s)	$2\varepsilon_A$ (mm/s)	B_A (T)	A_A (%)	δ_B (mm/s)	$2\varepsilon_B$ (mm/s)	B_B (T)	A_B (%)	A_A/A_B
1000 °C	0.25	0	49	45	0.36	0	52.3	27	1.67
1100 °C	0.25	0	49	52	0.36	0	52.3	48	1.08
1200 °C	0.25	0	49	50	0.36	0	52.3	50	1

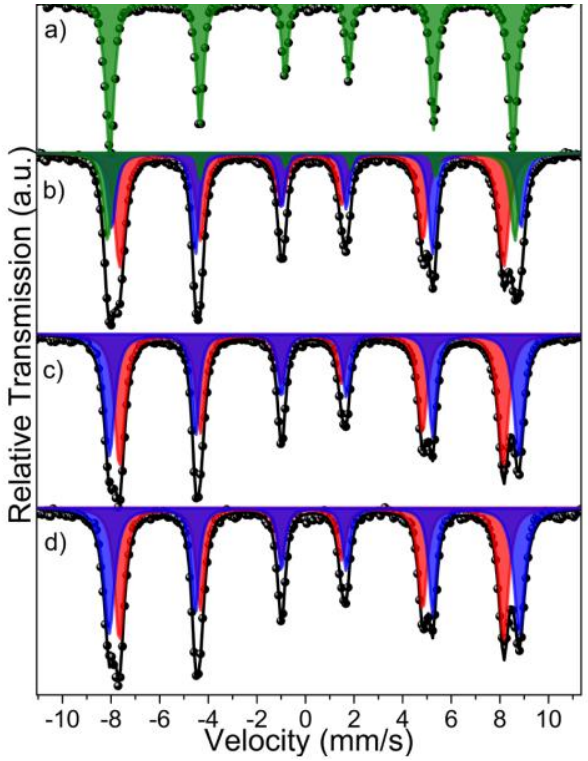

$$\frac{A_A}{A_B} = \left(\frac{f_A}{f_B}\right)\left(\frac{\lambda}{2-\lambda}\right)$$

where $\frac{f_A}{f_B}$ is the recoilless *f*-factors ratio for Fe^{3+} cations at (A) and [B] sites. Using equation (4) and considering $\frac{f_B}{f_A}$ at room temperature (RT) [24]; we found $\frac{A_A}{A_B} = 0$ for $\lambda = 0$, and $\frac{A_A}{A_B} = 0.92$ for $\lambda = 1$. Notice that the experimental values of $\frac{A_A}{A_B}$ reported in Table 2 are outside the range of expected

H. Salazar-Tamayo, K.E. García Tellez, C.A. Barrero Meneses. Materials Research. 2019; 22(5): e20190298

IR and Raman spectra of (a) the initial mixture of reactants, (b) 1000 °C, (c) 1100 °C and (d) 1200 °C.

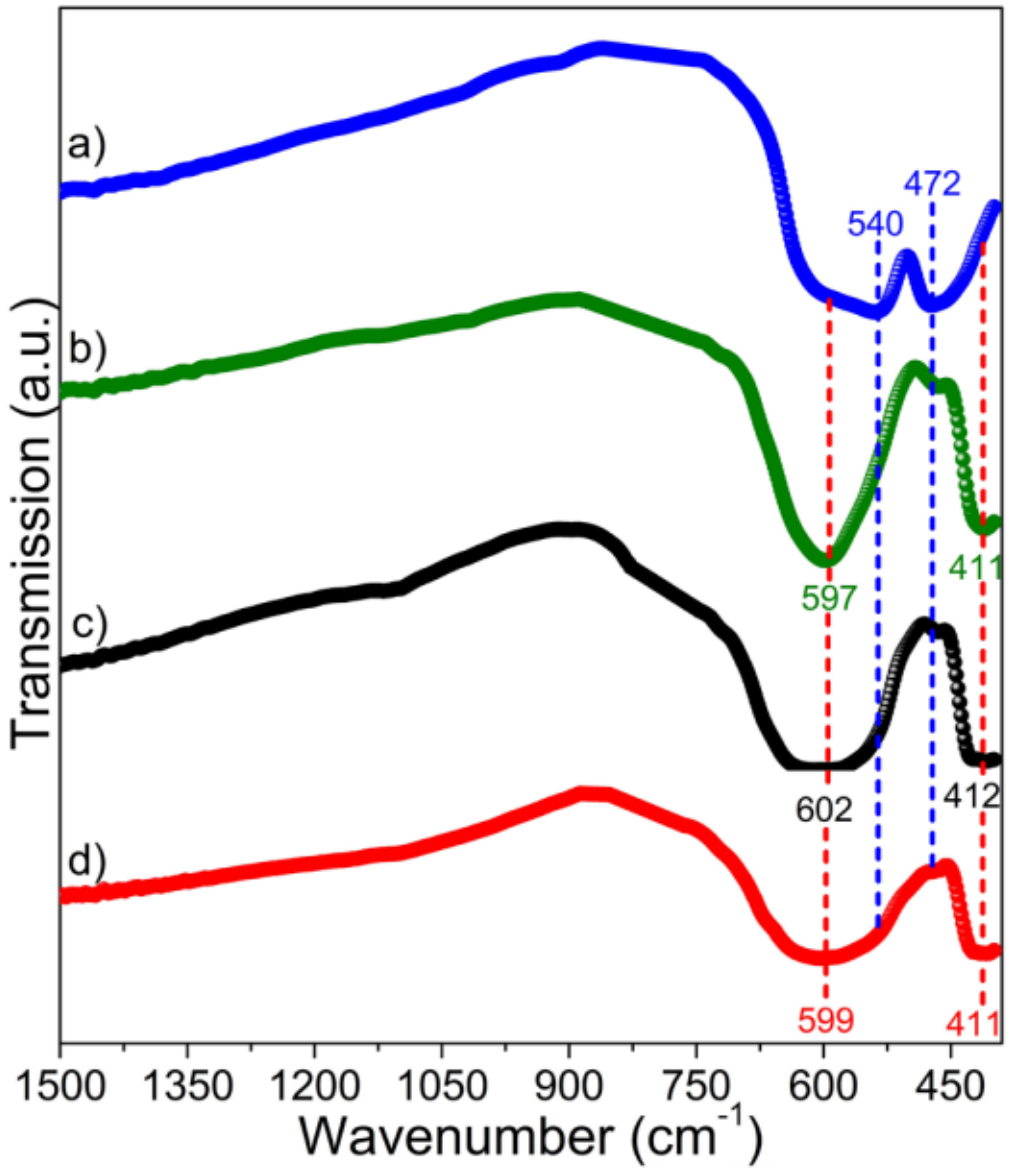

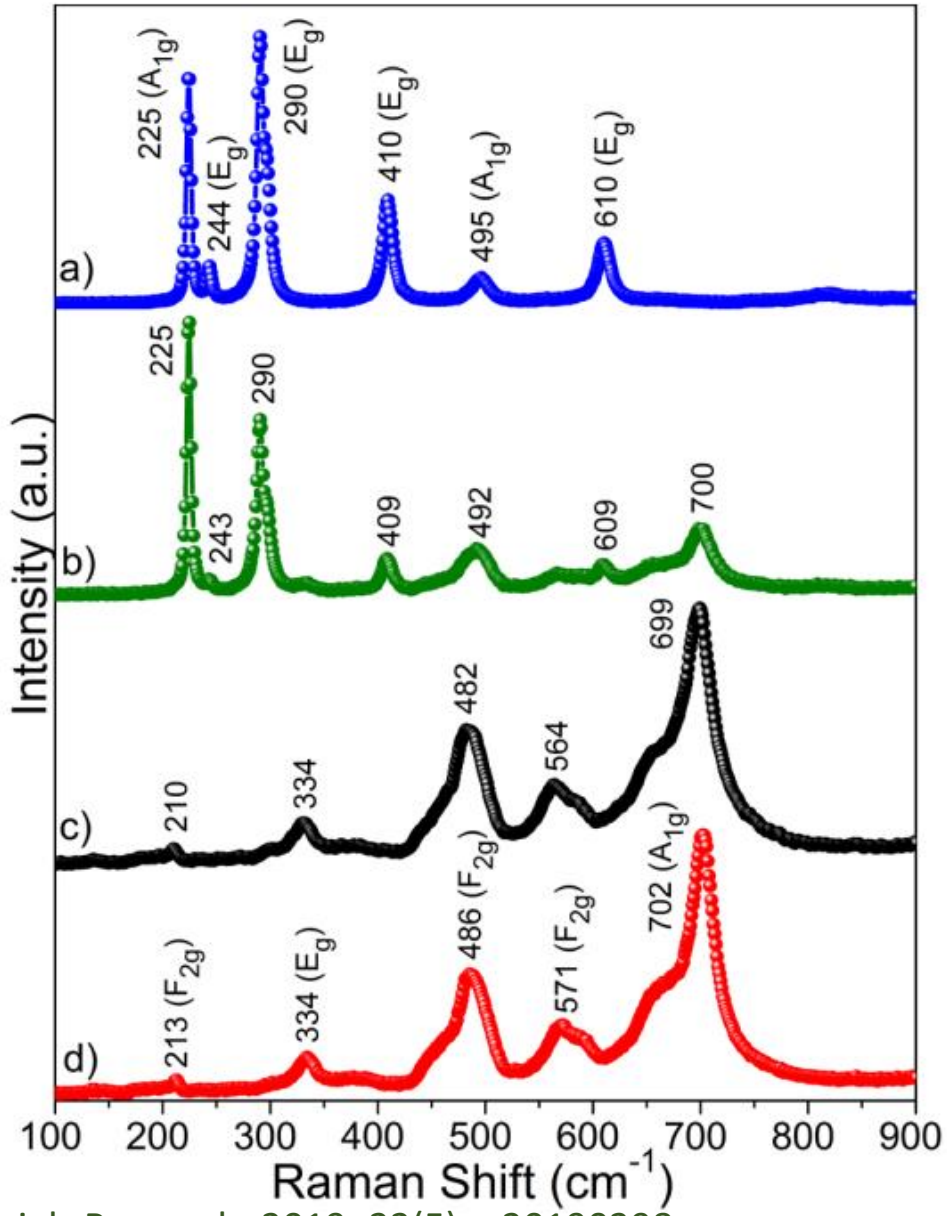

H. Salazar-Tamayo, K.E. García Tellez, C.A. Barrero Meneses. Materials Research. 2019; 22(5): e20190298

SEM micrograph and EDS spectra

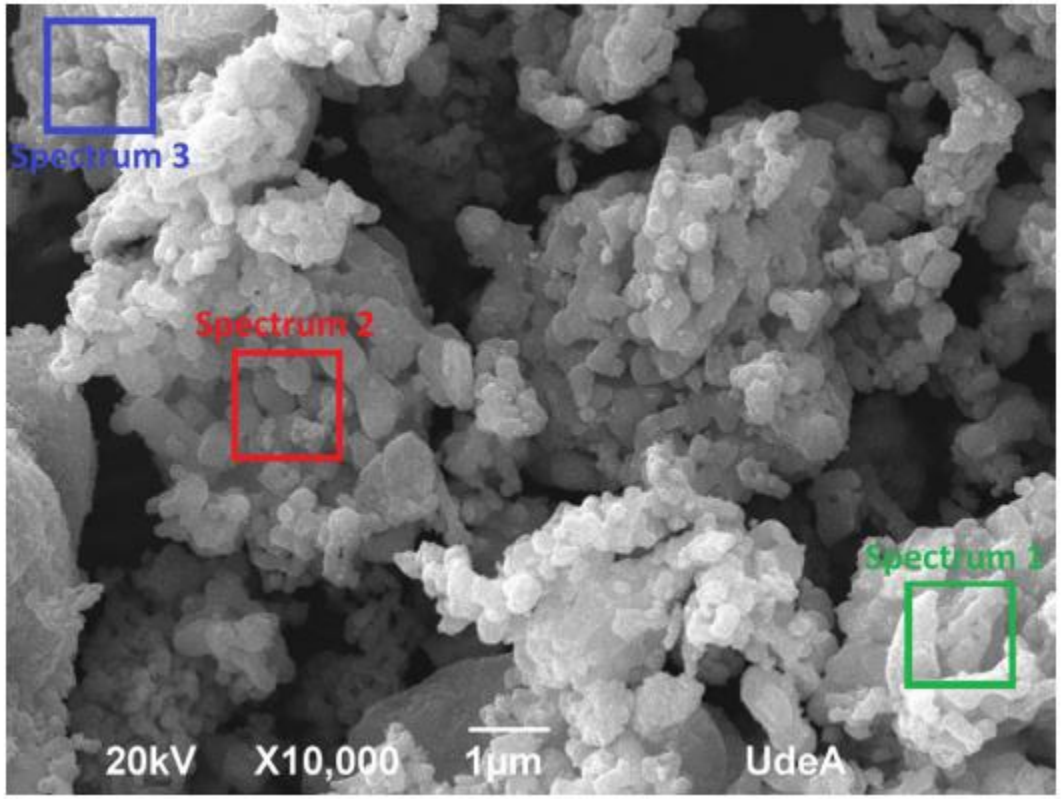

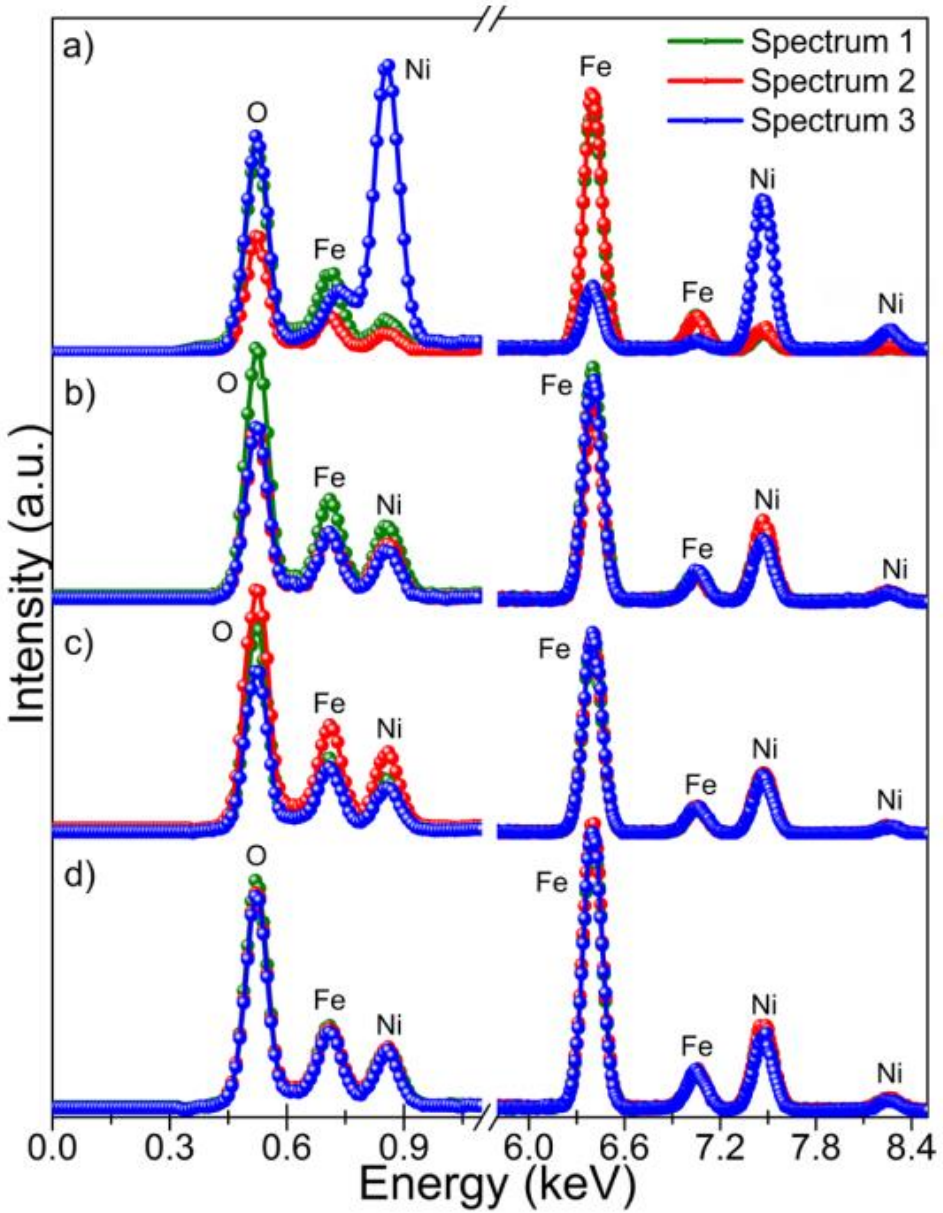

H. Salazar-Tamayo, K.E. García Tellez, C.A. Barrero Meneses. Materials Research. 2019; 22(5): e20190298

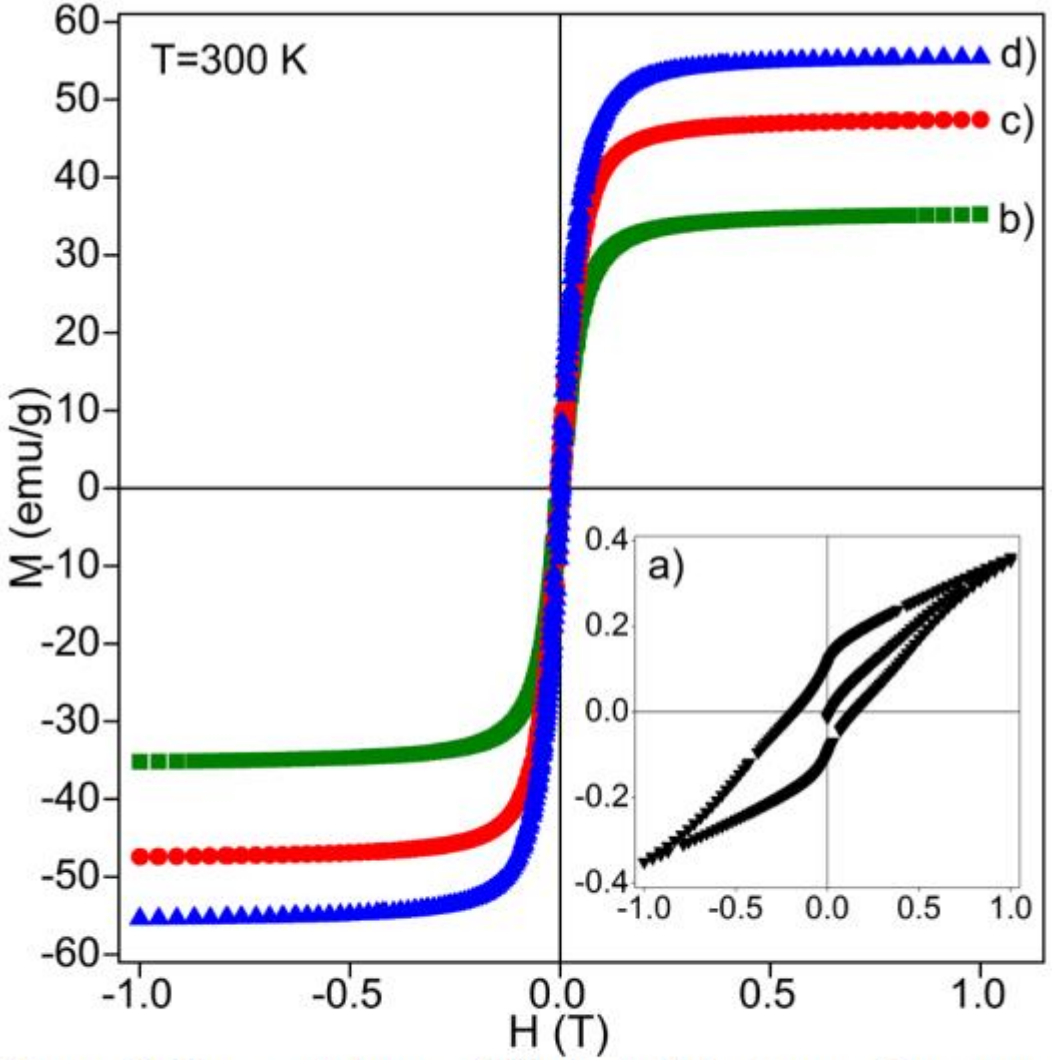

Figure 9. Hysteresis loops of (a) the initial mixture of reactants and of the samples submitted to heat treatments at (b) 1000 °C, (c) 1100 °C and (d) 1200 °C.

Table 3. Saturation magnetization (M_S), remanent magnetization (M_R) and coercive magnetic field (H_C) values obtained in the analysis of the hysteresis loops.

Sample	M_S (emu/g)	M_R (emu/g)	H_C (10^{-3} T)
Initial mixture	0.4	0.1	160
1000 °C	35.2	4.0	5.0
1100 °C	47.4	4.0	4.6
1200 °C	55.4	4.4	3.2

$$(Ni^{2+}_{1-\lambda}Fe^{3+}_{\lambda})_A[Ni^{2+}_{\lambda}Fe^{3+}_{2-\lambda}]_B\,O^{2-}_4 \qquad M_{the} = M_B - M_A$$

$$M_A = (1-\lambda)M_{Ni^{2+}} + \lambda M_{Fe^{3+}}$$

$$M_B = \lambda M_{Ni^{2+}} + (2-\lambda)M_{Fe^{3+}}$$

$$M_{the} = 2(4-3\lambda)\mu_B$$

$$(Ni^{2+}_{1-\lambda}\,Fe^{3+}_{\lambda})_A[\,Ni^{2+}_{\lambda-x}\,Fe^{3+}_{2-\lambda-y}\,V_{x+y}\,]_B\,O^{2-}_4$$

$$M_{the} = [2(4-3\lambda) - (2x+5y)]\mu_B$$

H. Salazar-Tamayo, K.E. García Tellez, C.A. Barrero Meneses. Materials Research. 2019; 22(5): e20190298

3. $Ni_{1-x}Zn_xFe_2O_4$ ($x \neq 0$)

Synthesis by solid state reaction

Step 1: Stoichiometric calculations.

Step 2: Mechanical Milling.

- Obtain a homogeneous mixture.
- Reduce the particle size.
- Increase the contact area between the reactants

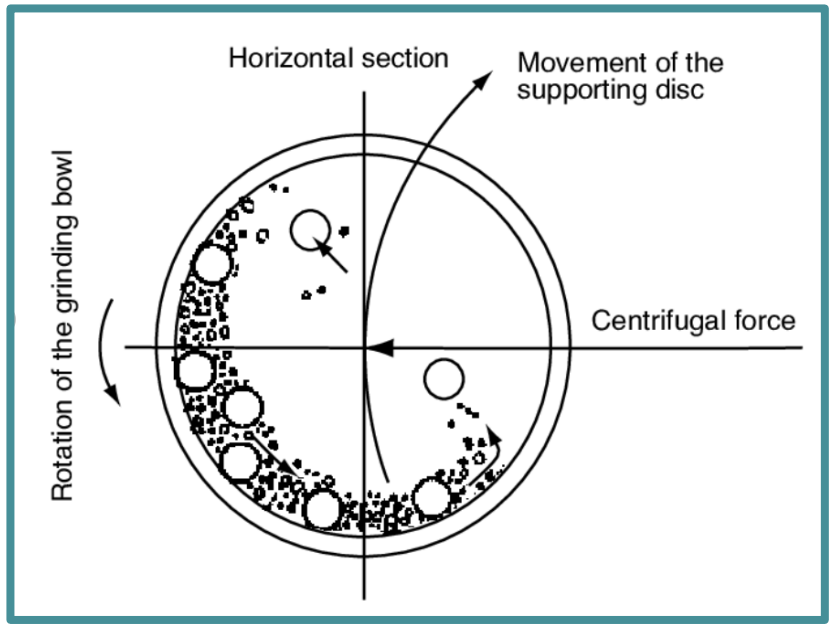

Step 3: Solid-State Reaction.

- Heating Rate: 2 ◦C/min.
- Maximum Temperature: 1250 ◦C.
- Thermal Treatment: 15 h.
- Cooling Rate: 10 ◦C/min.

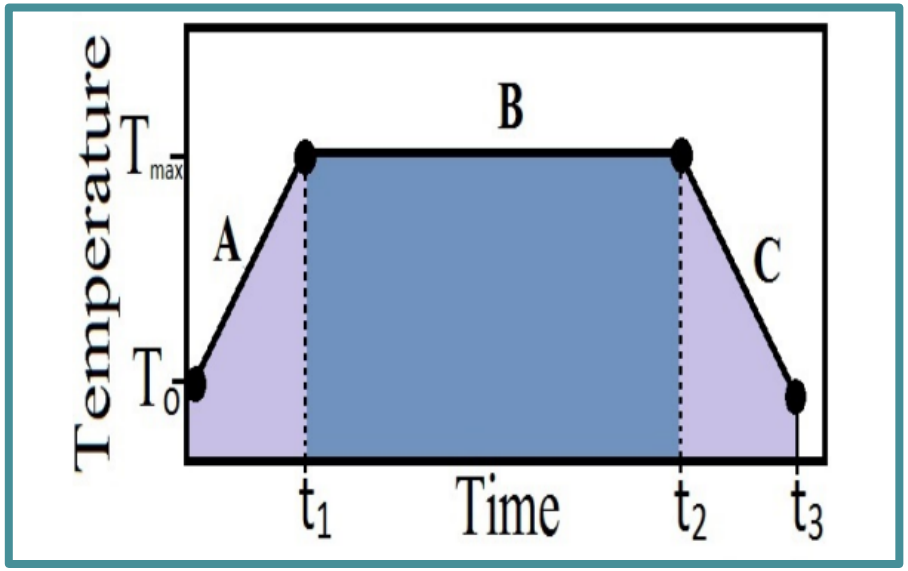

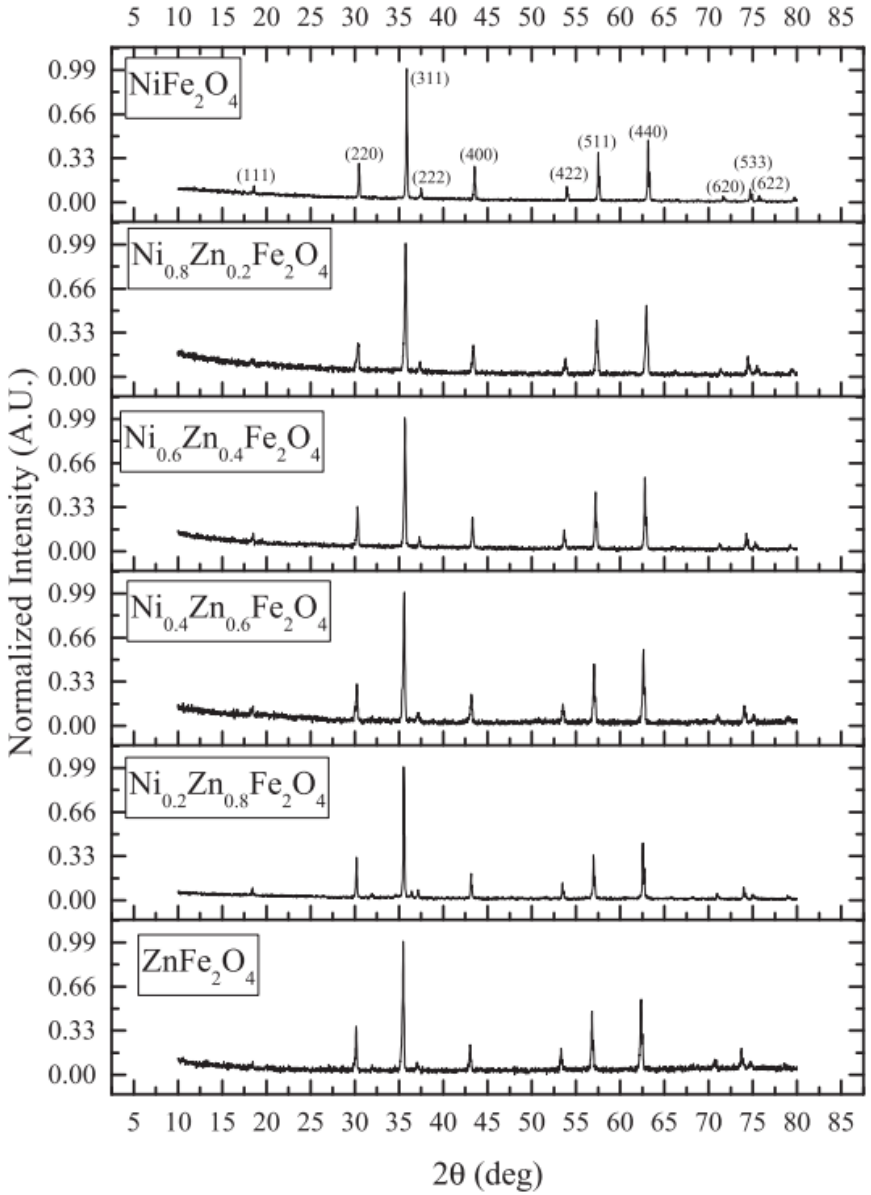

$$r_{Tetra} = |C_{Ni} r_{Ni^{2+}} + C_{Zn} r_{Zn^{2+}} + C_{Fe} r_{Fe^{3+}}|$$

$$r_{Octa} = 1/2\ |C_{Ni} r_{Ni^{2+}} + C_{Zn} r_{Zn^{2+}} + C_{Fe} r_{Fe^{3+}}|$$

$$a_{th} = \frac{8}{3\sqrt{3}}[(r_{Tetra} + r_o) + \sqrt{3}\,(r_{Octa} + r_o)]$$

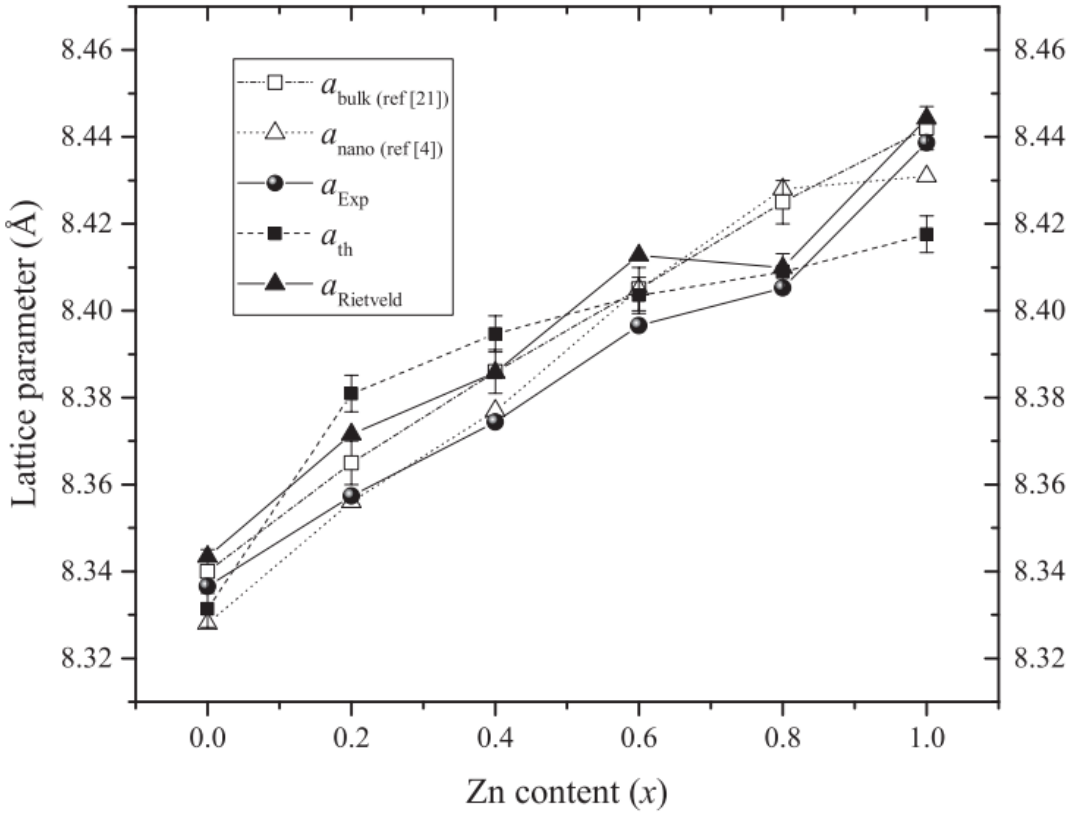

S.A. Mazen et al., Phys. Status Solidi A. 134 (1992) 263

C.A. Palacio Gómez, C.A. Barrero Meneses, A. Matute. Mater. Sci. & Engin. B 236–237 (2018) 48–55

Estimated cation distribution and X-ray intensity ratios for the $Ni_{1-x}Zn_xFe_2O_4$ ferrites.

x	Cation Distribution*	$I_{(220)} / I_{(440)}$		$I_{(400)} / I_{(220)}$		$\frac{Fe^{3+}\ Tetra}{Fe^{3+}\ Octa}$
		Obs.	Calc.	Obs.	Calc.	
0.0	$(Fe_{1.000})\ [Ni_{1.000}Fe_{1.000}]$	0.506	0.802	1.049	3.454	1.000
0.2	$(Ni_{0.512}Zn_{0.200}Fe_{0.288})\ [Ni_{0.288}Zn_{0.000}Fe_{1.712}]$	0.387	0.513	0.991	2.463	0.168
0.4	$(Ni_{0.456}Zn_{0.400}Fe_{0.144})\ [Ni_{0.144}Zn_{0.00}Fe_{1.856}]$	0.458	0.633	0.878	2.184	0.078
0.6	$(Ni_{0.380}Zn_{0.497}Fe_{0.123})\ [Ni_{0.020}Zn_{0.103}Fe_{1.877}]$	0.410	0.537	0.864	2.164	0.066
0.8	$(Ni_{0.153}Zn_{0.766}Fe_{0.081})\ [Ni_{0.047}Zn_{0.034}Fe_{1.919}]$	0.556	0.814	0.886	1.985	0.042
1.0	$(Zn_{1.000})[\ Fe_{2.000}]$	0.416	0.519	0.693	1.834	0.000

* Round () and square [ ] brackets denote, respectively, tetrahedral and octahedral coordination sites.

$$I_{hkl} = |F_{hkl}|^2 p L_p$$

$$L_p = \frac{1 + \cos^2 2\theta}{\sin^2 \theta \cos\theta}$$

$$f_a = (Zn_x) f_{Zn} + (Fe_{1-x}) f_{Fe}$$

$$f_b = (Ni_{1-x}) f_{Ni} + (Fe_{1+x}) f_{Fe}$$

$$F_{220} = -8 f_a$$

$$F_{400} = 8(f_a - 2f_b - 4f_o)$$

$$F_{440} = 8(f_a + 2f_b + 4f_o)$$

$$F_{422} = 8 f_a$$

$(Fe_{1-x}Zn_x)[Ni_{1-x}Fe_{1+x}]O_4$

$(Ni_\alpha Zn_{x-\beta} Fe_{1-x+\gamma})[Ni_{1-x-\alpha} Zn_\beta Fe_{1+x-\gamma}]O_4$

S.M. Patange et al. Phys. Status Solidi A 209 (2012) 347–352.
C.A. Palacio Gómez, C.A. Barrero Meneses, A. Matute. Mater. Sci. & Engin. B 236–237 (2018) 48–55

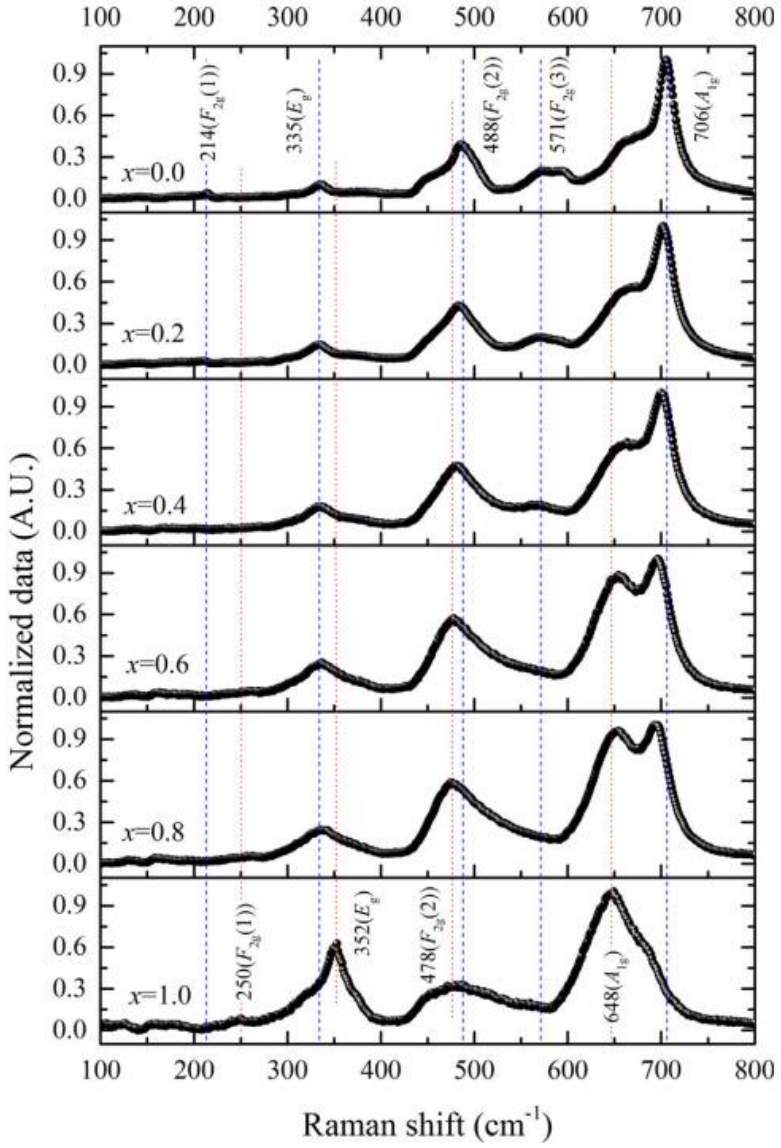

Location of the main Raman active modes for the $Ni_{1-x}Zn_xFe_2O_4$ (x = 0.0, 0.2, 0.4, 0.6, 0.8 and 1.0) ferrites.

Raman active mode	Raman shift (cm^{-1})					
	x = 0.0	x = 0.2	x = 0.4	x = 0.6	x = 0.8	x = 1.0
F_{2g}(1)	214.15	214.00	214.00	–	–	250.1
E_g	334.86	332.64	334.17	333.86	338.92	351.71
F_{2g}(2)	488.17	484.95	477.84	470.97	476.75	478.11
F_{2g}(3)	571.06	566.92	563.36	–	–	–
A_{1g}	705.94	703.14	701.35	660.18 and 696.83	656.20 and 695.62	648.06

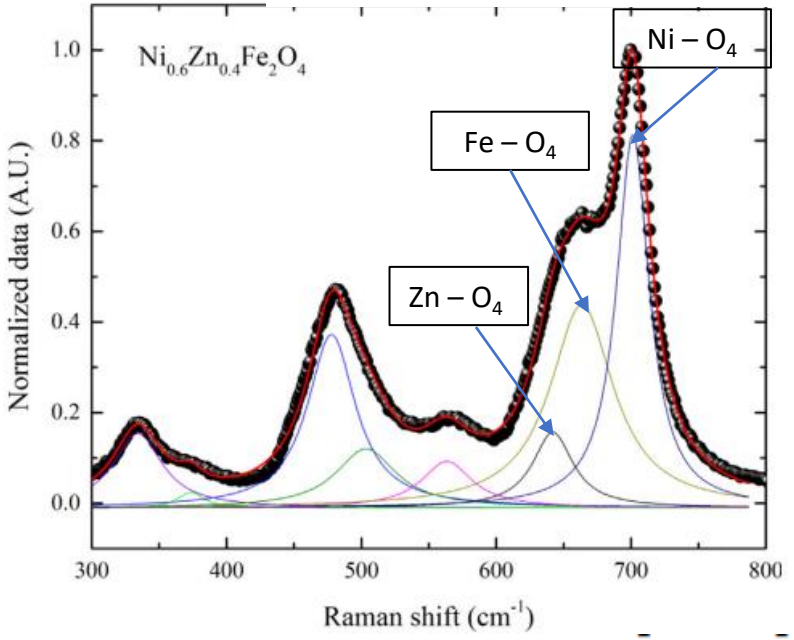

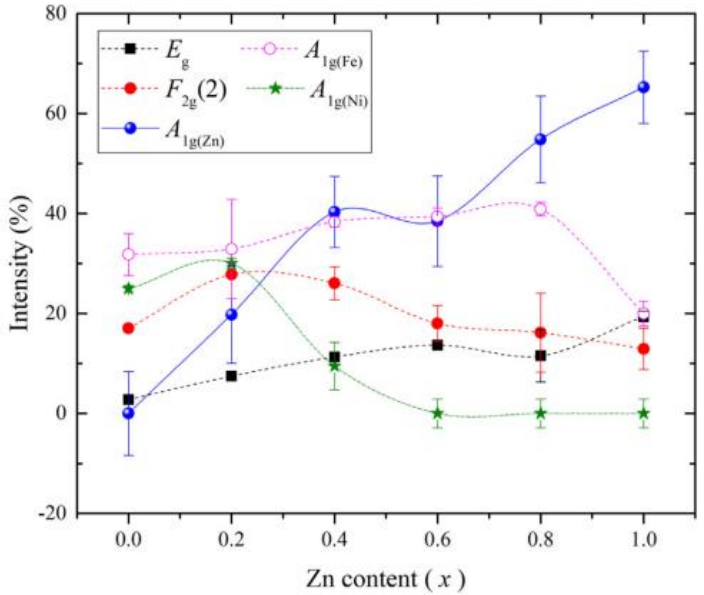

$$Zn_x = I_{Zn}/(I_{Zn} + I_{Ni} + I_{Fe})$$

Z.Ž. Lazarević, et al., Intern. Scholarly and Sci. Research & Innovation 9(8) 2015 1066.

C.A. Palacio Gómez, C.A. Barrero Meneses, J.A. Jaén. J. Magn. Magn. Mater. 505 (2020) 166710

RT

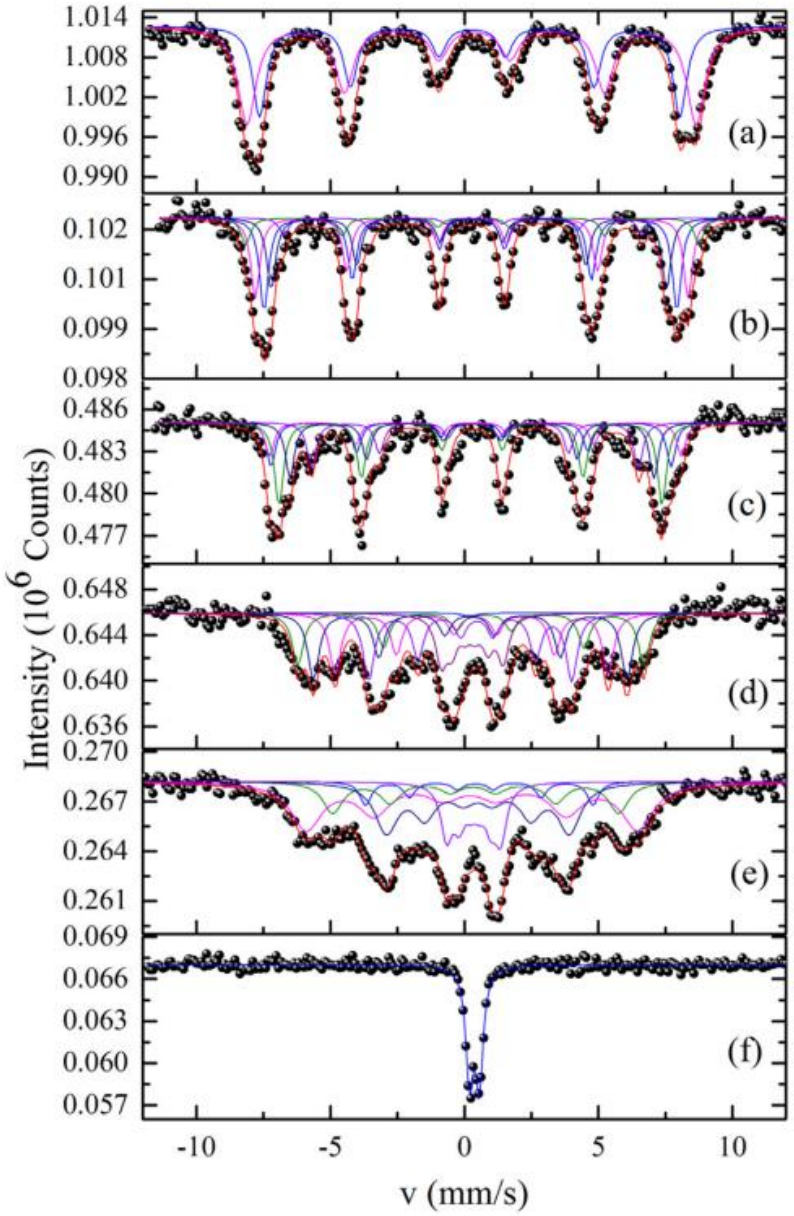

18 K

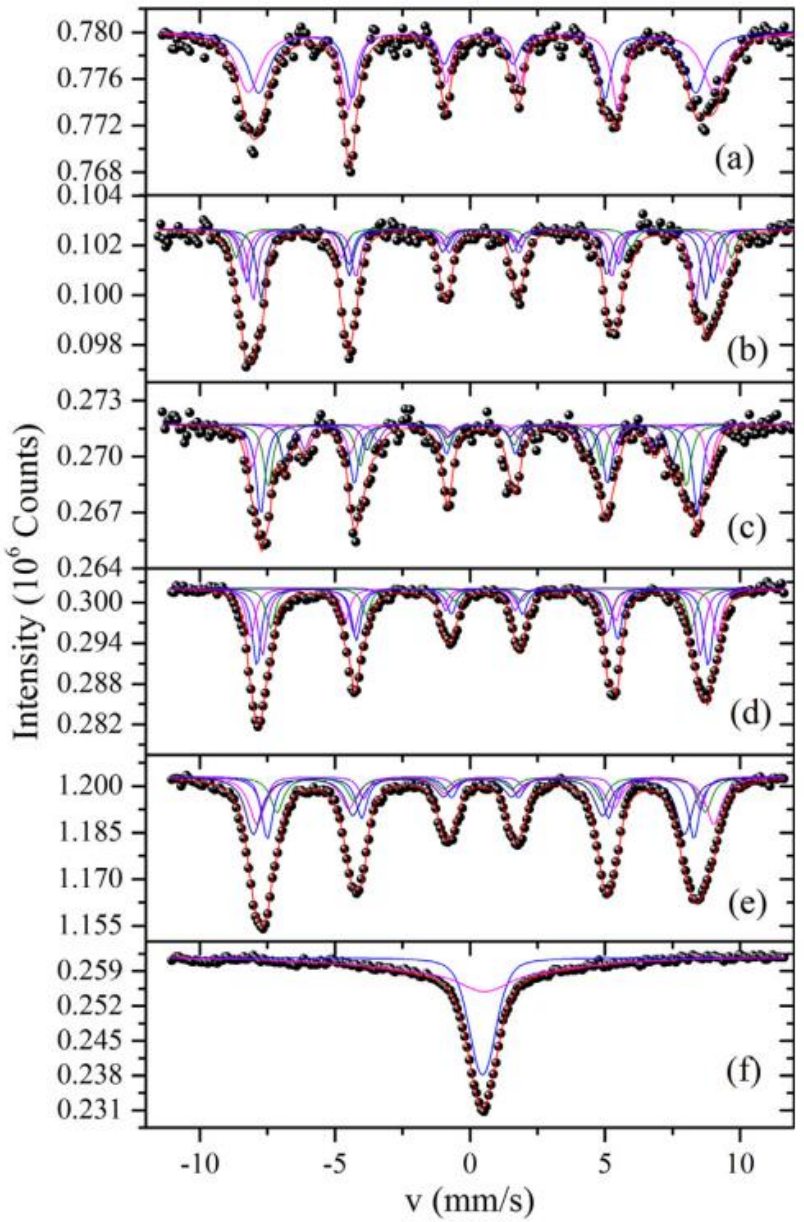

C.A. Palacio Gómez, C.A. Barrero Meneses, J.A. Jaén. J. Magn. Magn. Mater. 505 (2020) 166710

Based on Leung, Evans and Morrish, Phys. Rev. B. 8 (1973) 29

$$\langle B_{octa}(x,T)\rangle_{th} = B_{octa}(0,T) - \sum_{n=0}^{6} P(n,x)\Delta B_{octa}(n,T)$$

$$P(n,x) = \frac{6!}{n!(6-n)!}(x)^n(1-x)^{6-n}$$

$$\langle B_{octa}(x,T)\rangle_{th} = B_{octa}(0,T) - \sum_{n=0}^{6} nP(n,x)\Delta B_{octa}(1,T)$$

$$\Delta B_{octa}(1,T) = \frac{B_{octa}(0,T) - \langle B_{octa}(x,T)\rangle_{exp}}{\sum_{n=0}^{6} nP(n,x)}$$

ΔB_{octa} (1, 18K) = 0.9 ± 0.5 T

$Fe_A^{3+} - O^{2+} - Fe_B^{3+}$ superexchange interaction.

$(Zn_x^{2+}Fe_{1-x}^{3+})_A[Ni_{1-x}^{2+}Fe_{1+x}^{3+}]_BO_4^{2-}$

$$\left(\frac{A_{[B]}}{A_{(A)}}\right) = \left(\frac{1+x}{1-x}\right)\left(\frac{f_{[B]}}{f_{(A)}}\right) \qquad x = \frac{\left(\frac{A_{[B]}}{A_{(A)}}\right) - \left(\frac{f_{[B]}}{f_{(A)}}\right)}{\left(\frac{A_{[B]}}{A_{(A)}}\right) + \left(\frac{f_{[B]}}{f_{(A)}}\right)}$$

$(M_{1-\lambda}^{2+}Fe_{\lambda}^{3+})\ [M_{\lambda}^{2+}Fe_{2-\lambda}^{3+}]O_4^{2-}$

V. Šepelák et al., J. Alloy. Compd. 434–435 (2007) 776

$$\lambda = \frac{2\left(\frac{f_{[B]}}{f_{(A)}}\right)}{\frac{A_{[B]}}{A_{(A)}} + \frac{f_{[B]}}{f_{(A)}}}$$

Comparison of the Zn content (x values) at the tetrahedral sites as obtained from the three characterization techniques.

Nominal sample	X-Ray Diffraction*	Raman spectroscopy	18 K Mössbauer spectroscopy
$NiFe_2O_4$ (x = 0.0)	0.00	0.00	0.05
$Ni_{0.8}Zn_{0.2}Fe_2O_4$ (x = 0.2)	0.20	0.24	0.46
$Ni_{0.6}Zn_{0.4}Fe_2O_4$ (x = 0.4)	0.40	0.46	0.52
$Ni_{0.4}Zn_{0.6}Fe_2O_4$ (x = 0.6)	0.50	0.49	0.66
$Ni_{0.2}Zn_{0.8}Fe_2O_4$ (x = 0.8)	0.77	0.57	0.70
$ZnFe_2O_4$ (x = 1.0)	1.00	0.77	1.00

C.A. Palacio Gómez, C.A. Barrero Meneses, J.A. Jaén. J. Magn. Magn. Mater. 505 (2020) 166710
C.A. Palacio Gómez, C.A. Barrero Meneses, A. Matute. Mater. Sci. & Engin. B 236–237 (2018) 48–55

4. $Mg_{1-x}Zn_xFe_2O_4$

IR spectra of the mixed ferrites $Zn_xMg_{1-x}Fe_2O_4$.

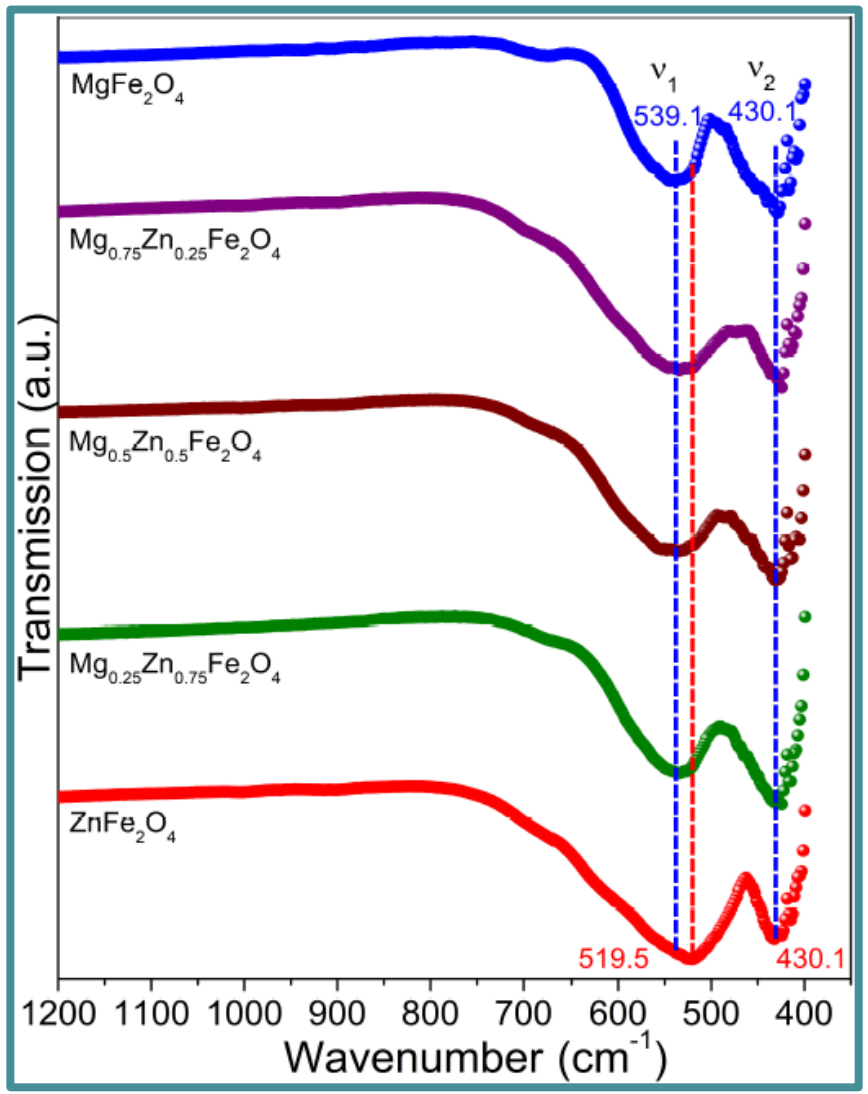

There are two main absorption bands that are unrelated to the reactants ZnO, MgO, and α-Fe_2O_3.

Sample	υ_1 (cm^{-1})	υ_2 (cm^{-1})
$MgFe_2O_4$	539.1	430.1
$Zn_{0.25}Mg_{0.75}Fe_2O_4$	535.1	430.1
$Zn_{0.5}Mg_{0.5}Fe_2O_4$	534.1	430.1
$Zn_{0.75}Mg_{0.25}Fe_2O_4$	532.3	430.1
$ZnFe_2O_4$	519.5	430.1

Infrared absorption bands of mixed ferrites $Zn_xMg_{1-x}Fe_2O_4$.

- υ_1 corresponds to stretching vibrations of the Fe^{3+}-O^{2-} bonds (A sites).
- υ_2 corresponds to metal-oxygen vibrations (B sites).

Fe-O bond length at tetrahedral sites → 1.901-1.976 Å

Fe-O bond length at octahedral sites → 2.045-2.032 Å

T. Tatarchuk, M. Myslin, I. Mironyuk, M. Bououdina, A.T. Pedziwiatr, R. Gargula, B.F. Bogacz, P. Kurzydlo. Synthesis, morphology, crystallite size and adsorption properties of nanostructured Mg-Zn ferrites with enhanced porous structure. Journal of Alloys and Compounds 819 (2020) 152945.

XRD patterns of mixed ferrites $Zn_xMg_{1-x}Fe_2O_4$ for different concentrations of Zinc .

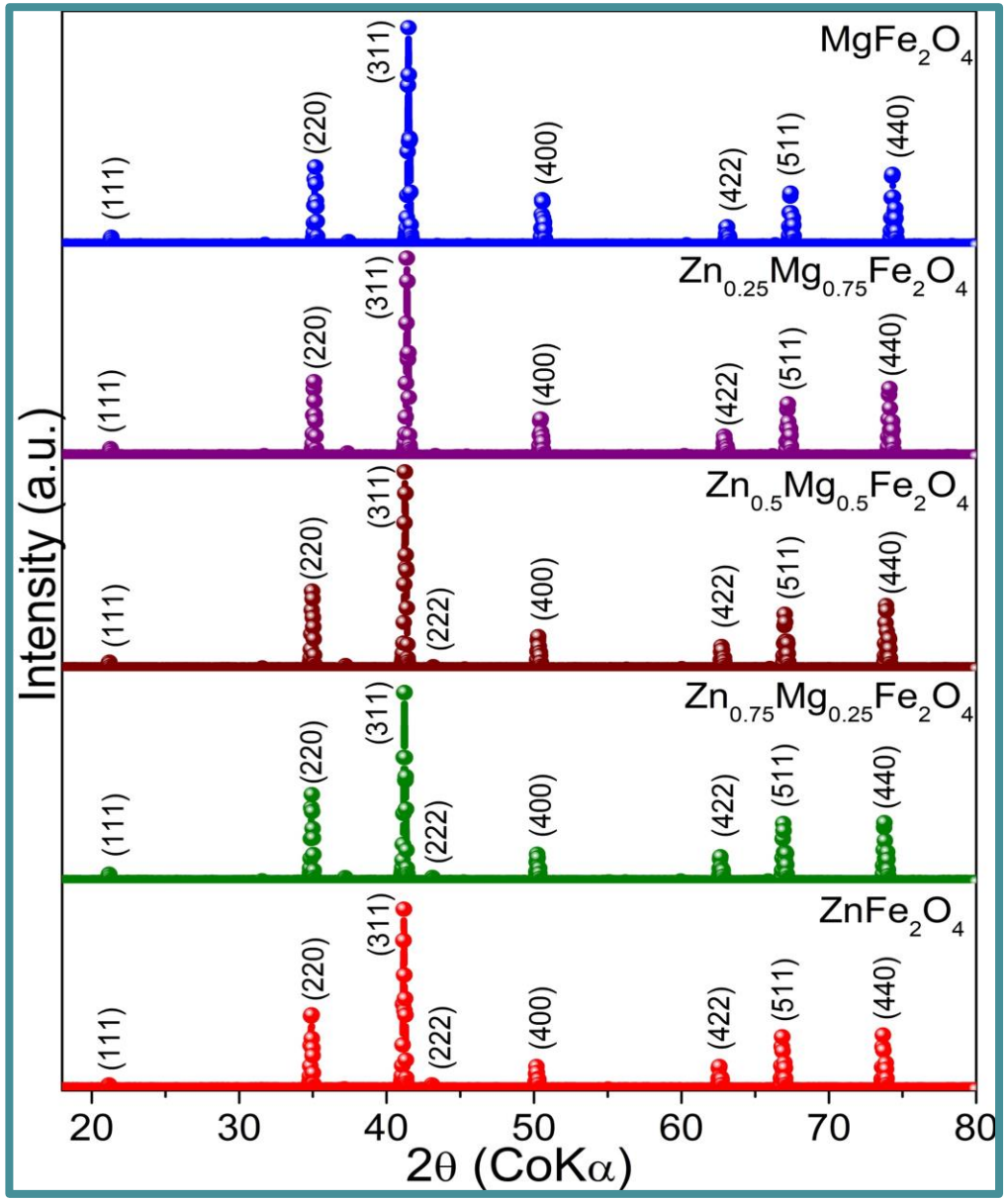

Displacement of the diffraction peaks (220) as a function of the Zn concentration.

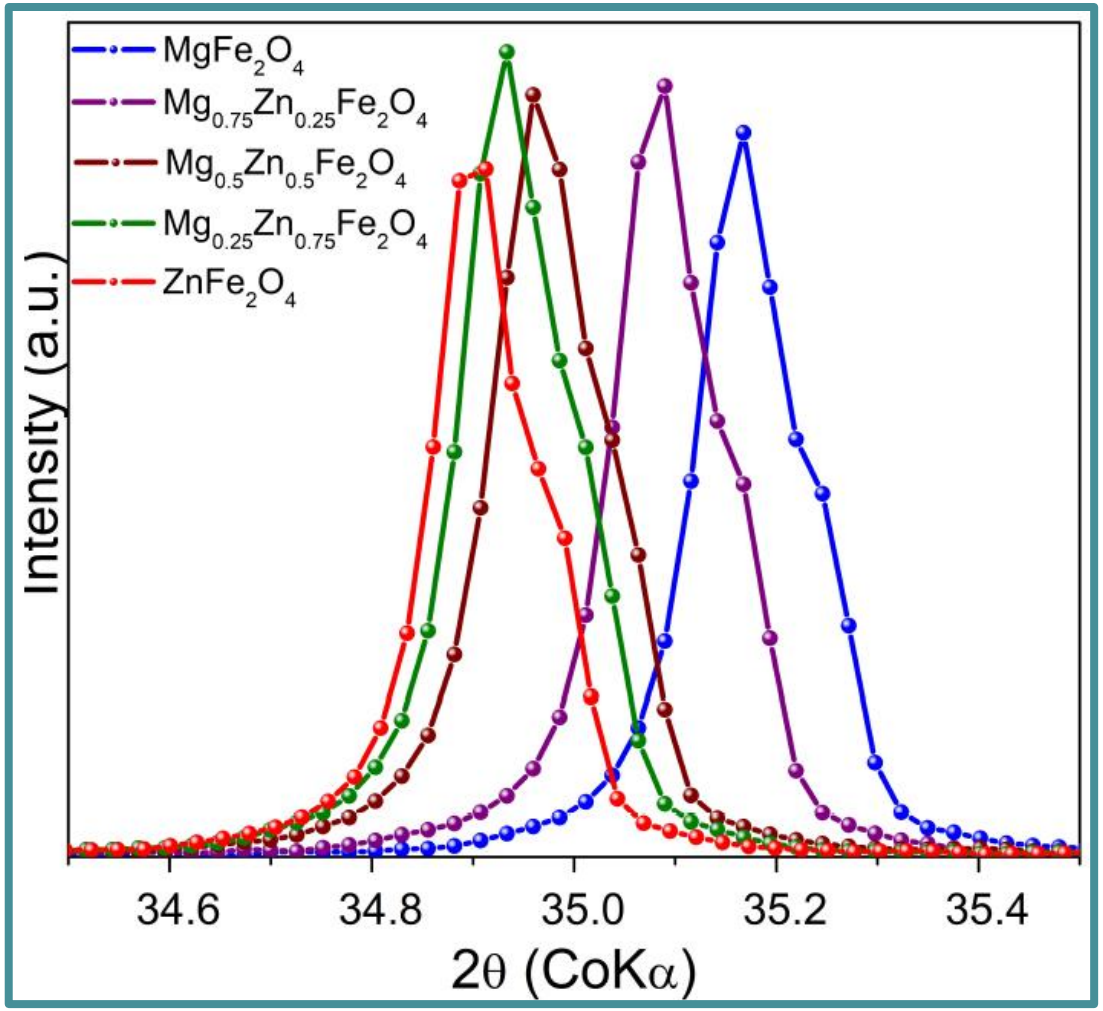

Determining lattice parameters

Rietveld analysis of mixed ferrites $Zn_xMg_{1-x}Fe_2O_4$ for different concentrations of Zinc.

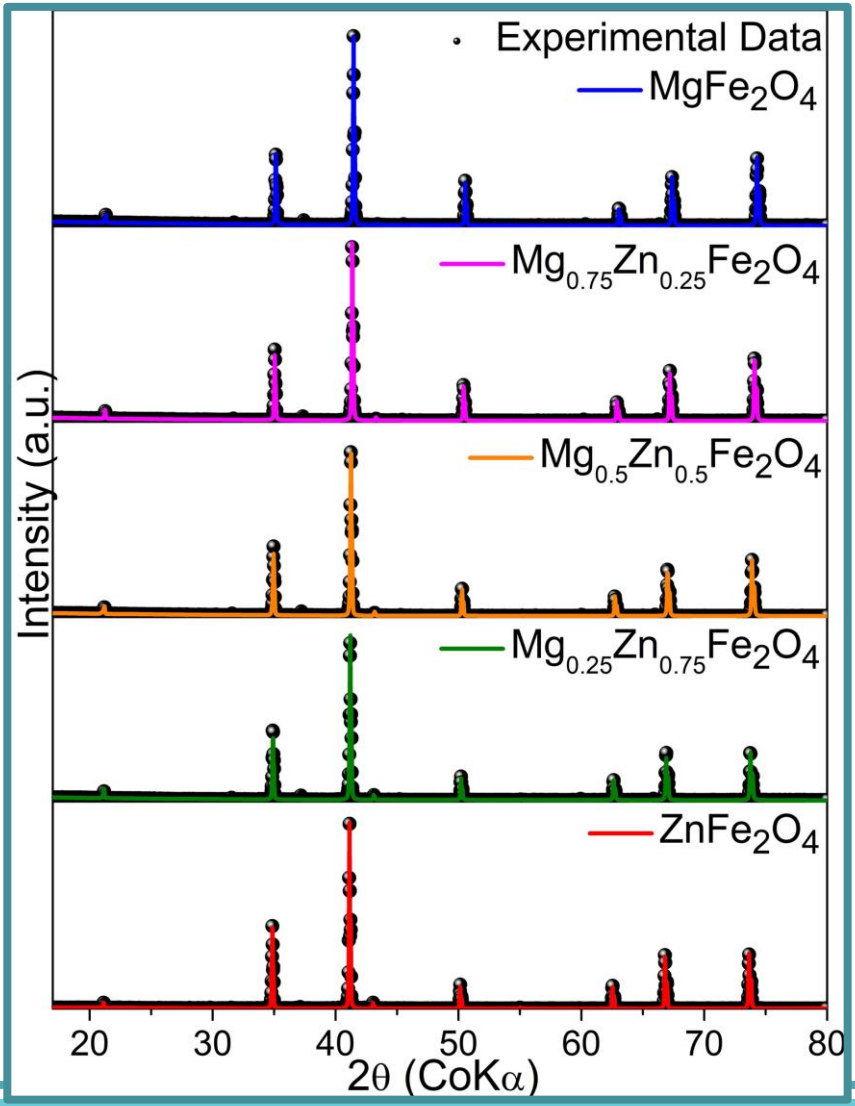

Rietveld analysis

The Rietveld method uses a least squares approach to refine a theoretical line profile until it matches the measured profile

Sample	Lattice parameter (Å)	Average crystallite size (Å)	Density ($g.cm^{-3}$)
$MgFe_2O_4$	8.379	762.68	4.51
$Zn_{0.25}Mg_{0.75}Fe_2O_4$	8.398	762.44	4.71
$Zn_{0.5}Mg_{0.5}Fe_2O_4$	8.418	762.11	4.91
$Zn_{0.75}Mg_{0.25}Fe_2O_4$	8.431	952.68	5.11
$ZnFe_2O_4$	8.442	761.89	5.32

Lattice parameter, average crystallite size and x-ray density of the mixed ferrites $Zn_xMg_{1-x}Fe_2O_4$, as a function of the Zn concentration.

Cation distribution

The cation distribution for the $Zn_xMg_{1-x}Fe_2O_4$ ferrites can be calculated

Theoretical lattice parameter

$$a_{th} = 8\frac{r_A + R_o + \sqrt{3}(r_B + R_o)}{3\sqrt{3}}$$

r_A and r_B are the cations radii of element at the tetrahedral and octahedral sites, respectively and R_o is the oxygen ion radius.

$$r_A = (C^A_{Mg^{2+}})(r_{Mg^{2+}}) + (C^A_{Zn^{2+}})(r_{Zn^{2+}}) + (C^A_{Fe^{3+}})(r_{Fe^{3+}})$$

$$r_B = \frac{(C^B_{Mg^{2+}})(r_{Mg^{2+}}) + (C^B_{Zn^{2+}})(r_{Zn^{2+}}) + (C^B_{Fe^{3+}})(r_{Fe^{3+}})}{2}$$

C^A and C^B are the ionic concentration at the tetrahedral and octahedral sites, respectively.
r_{Mg}^{2+}, r_{Zn}^{2+} and r_{Fe}^{3+} are the ionic radii of Mg^{2+}, Zn^{2+} and Fe^{3+} ions, respectively.

K.A. Mohammed, A.D.Al-Rawas, A.M. Gismelseed, A.Sellai, H.M. Widatallah, A. Yousif, M.E. Elzain, M. Shongwe. Infrared and structural studies of $Zn_xMg_{1-x}Fe_2O_4$ ferrites.

Cation distribution

$Zn_xMg_{1-x}Fe_2O_4$	Cation distributions
0.0	$(Mg_{0.11}Fe_{0.89})_A[Mg_{0.89}Fe_{1.11}]_BO_4$
0.25	$(Zn_{0.25}Mg_{0.263}Fe_{0.487})_A[Mg_{0.487}Fe_{1.513}]_BO_4$
0.5	$(Zn_{0.5}Mg_{0.254}Fe_{0.246})_A[Mg_{0.246}Fe_{1.754}]_BO_4$
0.75	$(Zn_{0.75}Mg_{0.114}Fe_{0.136})_A[Mg_{0.136}Fe_{1.864}]_BO_4$
1.0	$(Zn)_A[Fe_2]_BO_4$

Scanning Electron Microscopy (SEM)

SEM micrograph for the initial reactants mix at 5000x and 40000x magnifications.

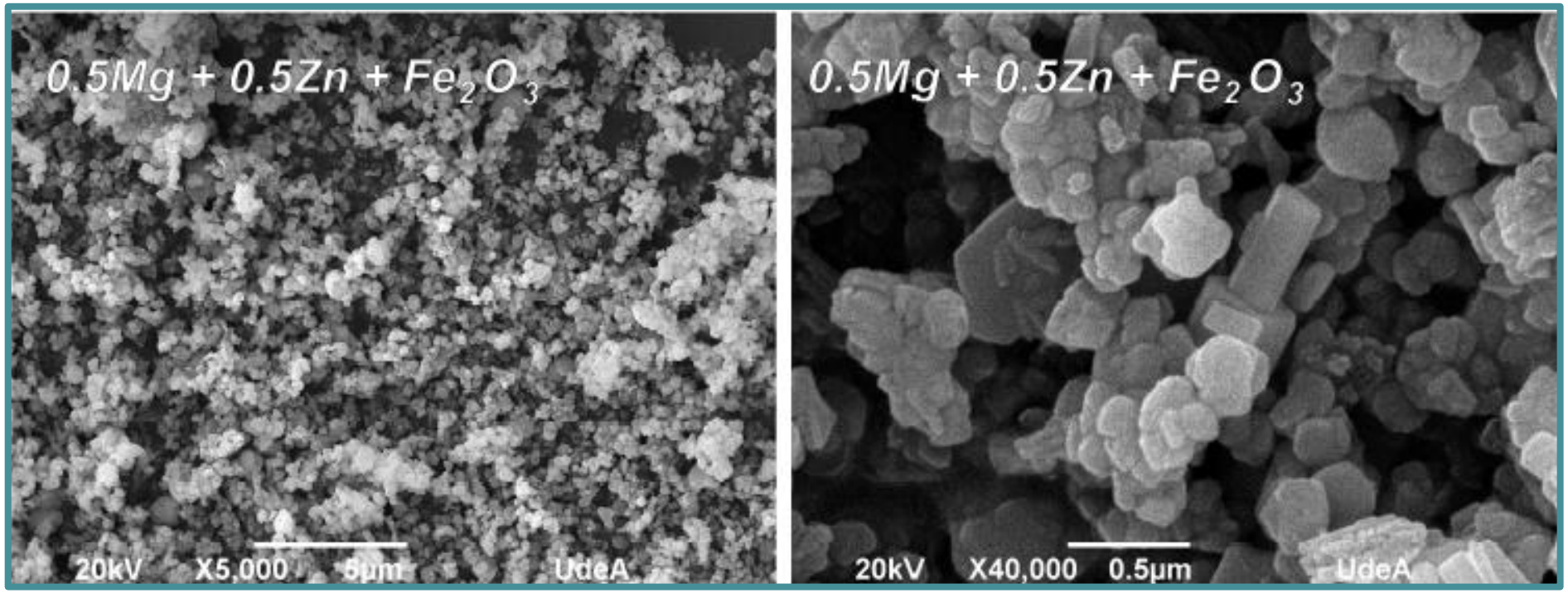

SEM micrograph of the mixed ferrites $Zn_xMg_{1-x}Fe_2O_4$ with 5000x magnification.

SEM micrograph of the mixed ferrites $Zn_xMg_{1-x}Fe_2O_4$ with 10000x magnification.

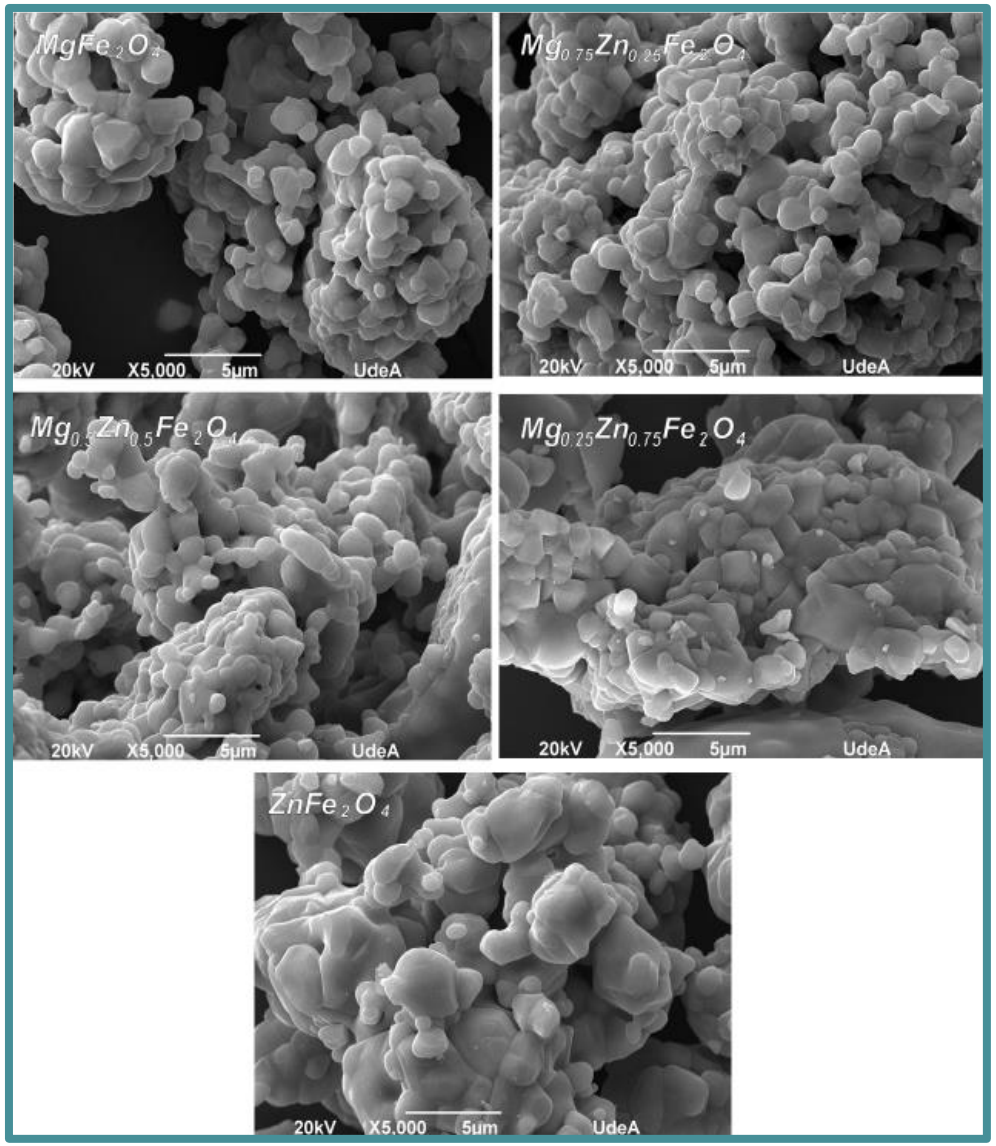

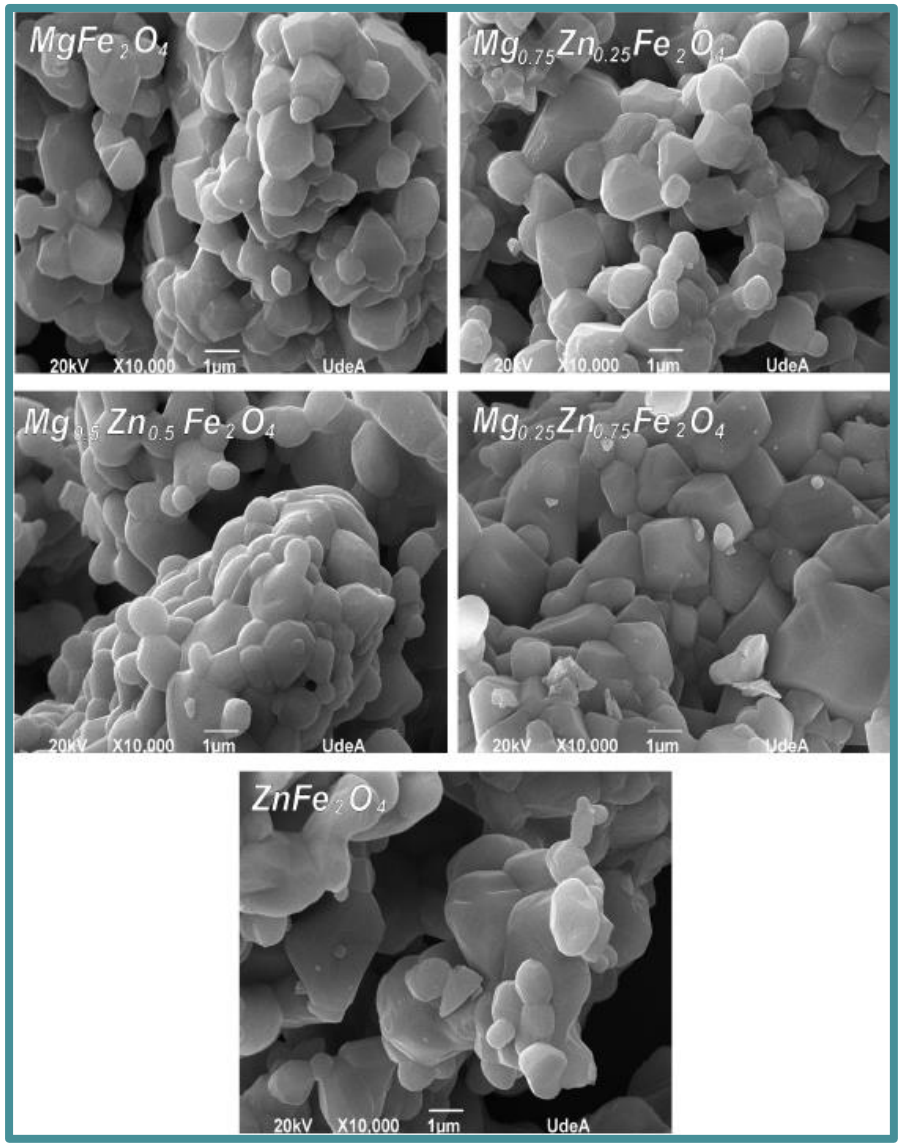

Mössbauer spectra of mixed ferrites $Zn_xMg_{1-x}Fe_2O_4$.

x = 0

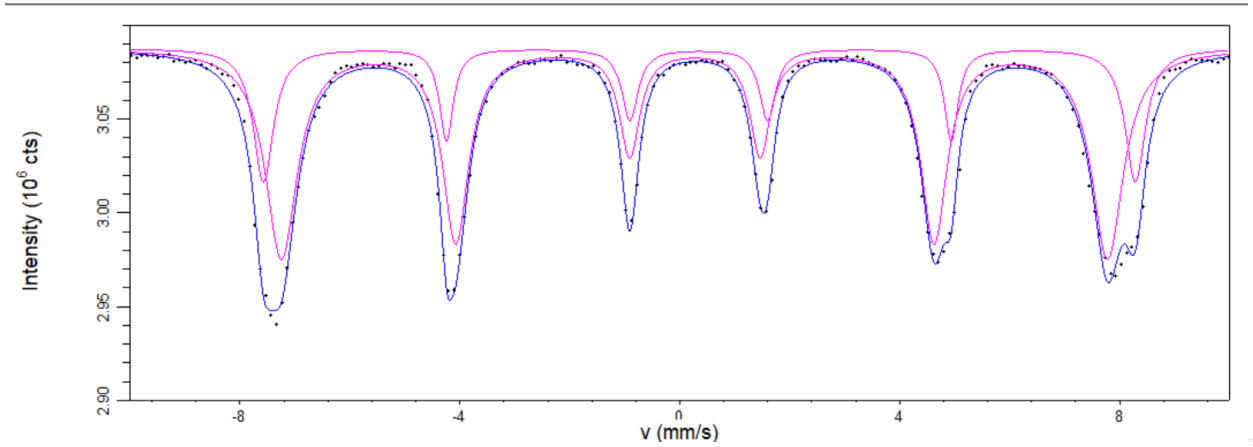

x = 0. 5

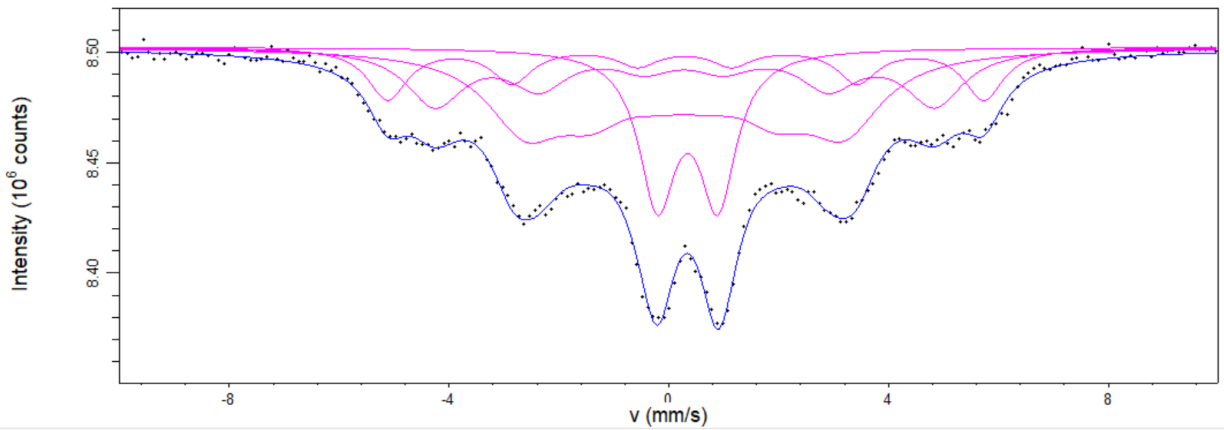

x = 0.25

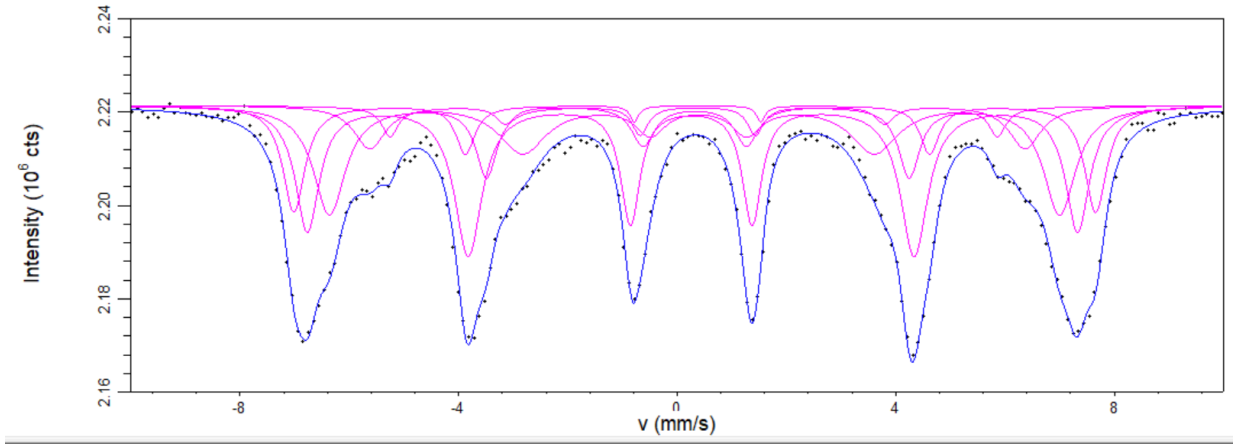

x = 1

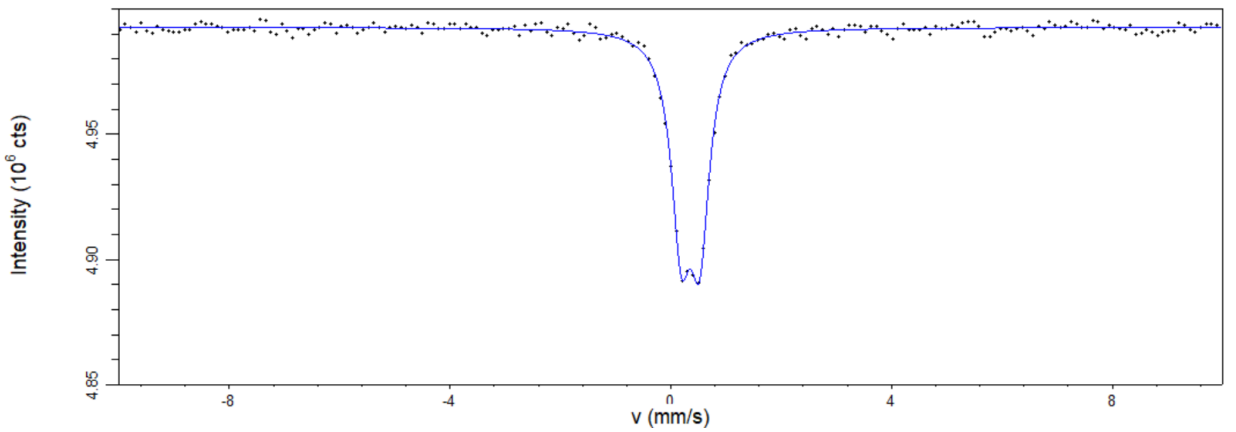

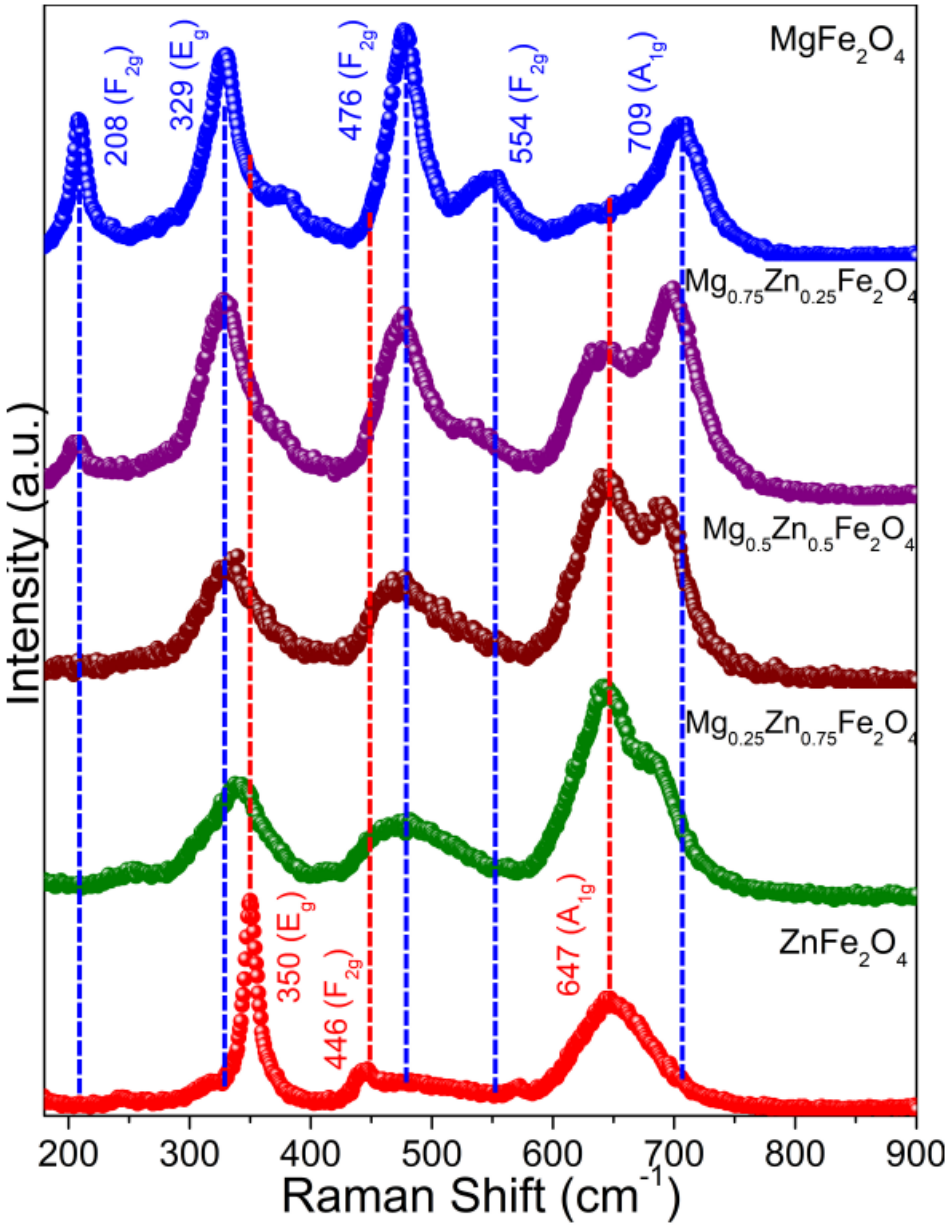
MgFe2O4
Mg0.75Zn0.25Fe2O4
Mg0.5Zn0.5Fe2O4
Mg0.25Zn0.75Fe2O4
ZnFe2O4
208 (F2g)
329 (Eg)
476 (F2g)
554 (F2g)
709 (A1g)
350 (Eg)
446 (F2g)
647 (A1g)
Intensity (a.u.)
Raman Shift (cm-1)
200
300
400
500
600
700
800
900

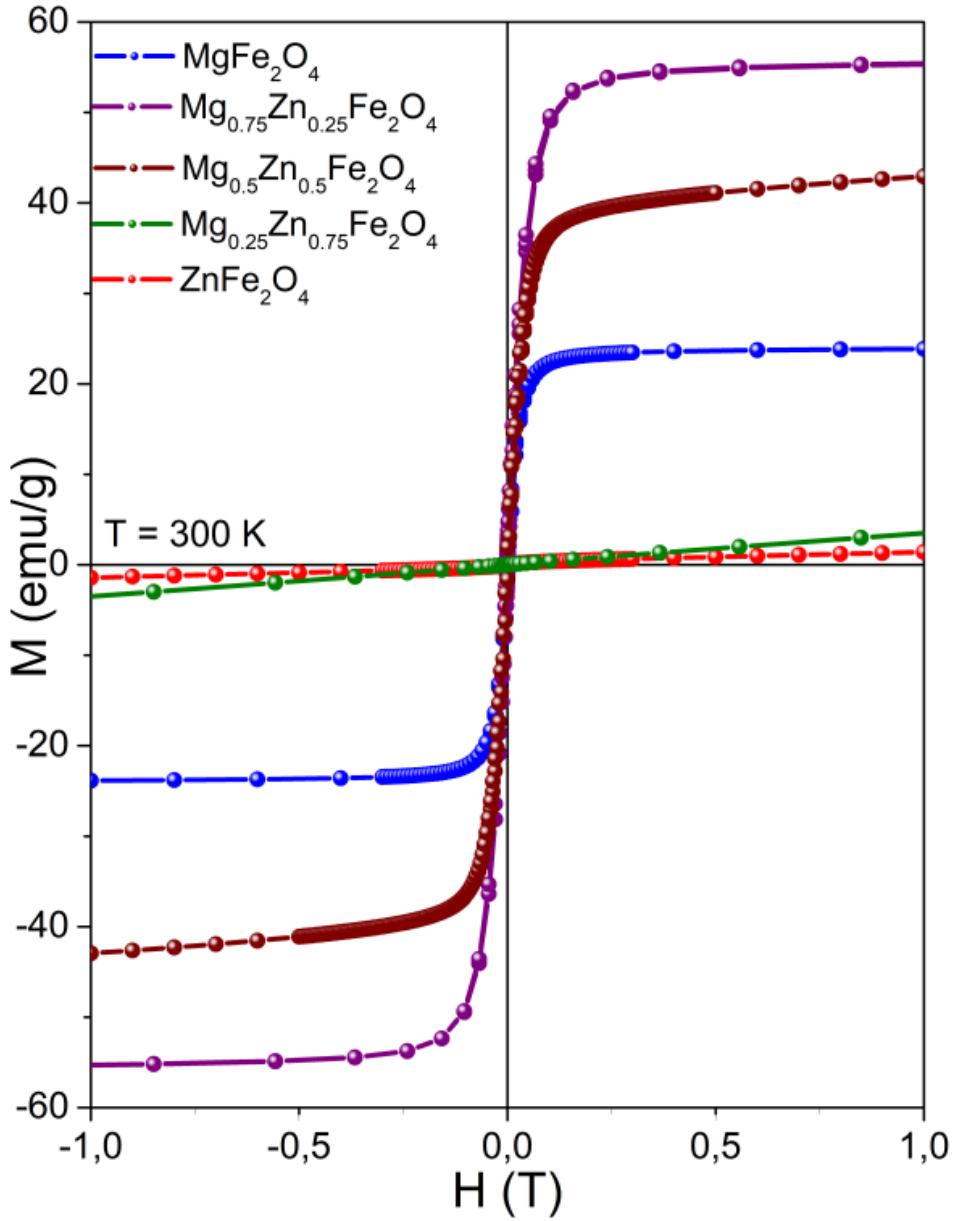
MgFe2O4
Mg0.75Zn0.25Fe2O4
Mg0.5Zn0.5Fe2O4
Mg0.25Zn0.75Fe2O4
ZnFe2O4
T = 300 K
M (emu/g)
H (T)
60
40
20
0
-20
-40
-60
-1,0
-0,5
0,0
0,5
1,0

SUMMARY

We proposed a simple formula to directly determining the 300 K relative recoilless *f*-factors for the two A and B sites of ferrites. We applied this methodology to three ferrites: $NiFe_2O_4$, $FeFe_2O_4$, and $MgFe_2O_4$. The method can be applied to all ferrites at any temperature.

Defective spinel $NiFe_2O_4$ is formed at 1000 °C, and as the temperature increases, the defects gradually disappear. Neither cation reordering phenomena nor possible evaporation of chemical elements were the dominant effects to account for the results. The results can be explained if it is assumed that [B]-sites cation vacancies are gradually filled with cations as temperature of heat treatment increases.

The synthesis of the $Zn_xM_{1-x}Fe_2O_4$ (with M = Ni and Mg) materials and the formation of the spinel structure were confirmed using X-ray diffraction, infrared spectroscopy, scanning electron microscopy and Mössbauer spectroscopy techniques. The presence of Zn^{2+} cations in the tetrahedral site causes a certain amount of Fe^{3+} cations to migrate from site A to site B, which causes important changes in the physico-chemical properties of the samples.

Determination of the stoichiometry of the ferrites were compared by using three different techniques: XRD, Raman and Mössbauer.

¡THANKS!

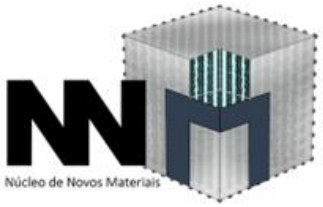

LACAME'22

XVII Latin American Conference On The Applications Of The Mössbauer Effect